Calculation of Metallocene Ionization Potentials via Auxiliary Field Quantum Monte Carlo: Towards Benchmark Quantum Chemistry for Transition Metals

Benjamin Rudshteyn,[†,‖] John L. Weber,[†] Dilek Coskun,[†] Pierre A. Devlaminck,[†] Shiwei Zhang,[*,‡,¶] David R. Reichman,[*,†] James Shee,[*,§] and Richard A. Friesner[*,†]

†*Department of Chemistry, Columbia University, 3000 Broadway, New York, NY, 10027*

‡*Center for Computational Quantum Physics, Flatiron Institute, 162 5th Avenue, New York, NY 10010*

¶*Department of Physics, College of William and Mary, Williamsburg, VA 23187*

§*Department of Chemistry, University of California, Berkeley, CA 94720*

‖*Present Address: Schrödinger Inc., 1540 Broadway 24th Floor New York, NY, 10036, USA*

E-mail: szhang@flatironinstitute.org; drr2103@columbia.edu; jshee@berkeley.edu; raf8@columbia.edu

Abstract

The accurate *ab initio* prediction of ionization energies is essential to understanding the electrochemistry of transition metal complexes in both materials science and biological applications. However, such predictions have been complicated by the scarcity of gas-phase experimental data, the relatively large size of the relevant molecules, and the presence of strong electron correlation effects. In this work, we apply all-electron phaseless auxiliary-field quantum Monte Carlo (ph-AFQMC) utilizing multi-determinant trial wavefunctions to six metallocene complexes to compare the computed adiabatic and vertical ionization energies to experimental results. We find the ph-AFQMC mean averaged errors (MAE) of 1.69 ± 1.02 kcal/mol for the adiabatic energies and 2.85 ± 1.13 kcal/mol for the vertical energies. This significantly outperforms density functional theory (DFT), which has MAE's of 3.62 to 6.98 and 3.31 to 9.88 kcal/mol, as well as a localized coupled cluster approach (DLPNO-CCSD(T_0) with moderate PNO cut-offs), which has MAEs of 4.96 and 6.08 kcal/mol, respectively. We also test the reliability of DLPNO-CCSD(T_0) and DFT on acetylacetonate (acac) complexes for adiabatic energies measured in the same manner experimentally, and find higher MAE's, ranging from 4.56 kcal/mol to 10.99 kcal/mol (with a different ordering) for DFT and 6.97 kcal/mol for DLPNO-CCSD(T_0), indicating that none of these approaches can be considered benchmark methods, at least for these complexes. We thus demonstrate that ph-AFQMC should be able to handle metallocene redox chemistry with the advantage of systematically improvable results. By utilizing experimental solvation energies, we show that accurate reduction potentials in solution can be obtained.

Introduction

Quantum chemical methodology has made tremendous progress in both accuracy and computational efficiency during the past three decades.[1] The early 1990's saw revolutionary improvements in density functional theory (DFT) via gradient corrected and then hybrid formalisms, yielding remarkable reductions in the mean unsigned errors in predicted bond

energies of organic molecules as, for example, assessed using Pople's G3 database, from 85.27 kcal/mol (LDA) to 4.27 kcal/mol (B3LYP).[2] In parallel, wavefunction based *ab initio* techniques, in particular the CCSD(T) variant of coupled cluster theory, enabled the attainment of chemical accuracy (∼1 kcal/mol MAE) for these same data sets, albeit at a much higher computational cost.[3]

Since these initial breakthroughs, reductions driven by Moore's law of the cost/performance of computing, coupled with continued progress on theoretical models, algorithms, and software implementations, have greatly expanded the domain of applicability of both the DFT and wavefunction based approaches. Thousands of new DFT functionals have been created and tested, a number of which have demonstrated significant robustness in addressing many of the outlier cases which had plagued PBE,[4] B3LYP,[5–7] and related models.[8–12]

It is now possible to routinely apply DFT calculations to systems containing hundreds to thousands of atoms, including transition metal containing species, and quite often obtain chemically accurate and useful results. The development of localized coupled cluster formulations by a number of research groups (e.g. those of Werner[13,14] and Neese[15–20]) has made it possible to routinely perform CCSD(T) computations for systems containing tens to hundreds of atoms; in many cases, the localization approximations have been shown to have a minimal effect on the accuracy that can be achieved. Furthermore, via the use of mixed quantum mechanics/molecular mechanics algorithms, DFT based approaches can be applied to very large and complex systems such as enzymes,[21] and corrected (if necessary) by CCSD(T) cluster calculations on the reactive core of the system.[22]

The accuracy of both DFT and CCSD(T) for transition metals has been a much more controversial topic than their performance for typical organic systems. CCSD(T) yields highly precise results for transition metal atoms (for example for ionization energies),[23] but the chemical accuracy of this approach as well as DFT for diatomic molecular bond dissociation energies has remained contentious.[24–30] Recently, Hait et. al. examined the convergence of coupled cluster to a theoretical benchmark for a series of 69 3d transition

metal oxides, sulfides, carbides, and nitrides, albeit with small basis sets. They found that higher orders of coupled cluster, e.g. CCSDTQ, are often needed to achieve chemical accuracy, and that sometimes the CCSD(T) result is fortuitously better than the CCSDT(Q) result. Such errors were not necessarily correlated with multireference character. DFT results vary widely depending upon the functional that is used and the specific systems being treated. In many cases, the results for metal complexes are surprisingly accurate, and at the very least enable considerable insight to be obtained into reaction mechanisms. However, no one has yet rigorously demonstrated, using large and diverse data sets, that any DFT functional achieves reliable performance for transition metal containing systems even at the level of "near-chemical" accuracy (3-4 kcal/mol errors). The problem is in part due to the paucity of high quality gas phase experimental data for transition metal containing systems,[24,31–40] in contrast to organic molecules where hundreds to thousands of such data points are available for a variety of important thermochemical properties. Additionally, calculations involving solvent and other complicating factors (which typically necessitate the use of heavily parametrized models[41,42]), or reference reactions, which can be used to take advantage of error cancellation,[43,44] make it extremely difficult to render an accurate assessment of the performance of DFT based on a small data set of condensed phase experiments. Furthermore, the experiments can be difficult to interpret, an issue compounded by the fact that many transition metal species have a number of close-lying low-energy spin states. For example, assigning ground and vertical state multiplicity in photoelectron spectroscopy can be complicated.[45]

In a series of recent publications, we have made progress in addressing many of the above problems related to transition metal quantum chemistry via the use of auxiliary field quantum Monte Carlo (AFQMC) calculations. The AFQMC methodology, developed originally in the physics community,[46,47] has a number of potential advantages as compared to traditional wavefunction based *ab initio* methods, including a more favorable formal scaling with system size (N) of N^3 (with planewaves[46]) or N^4 (with Gaussian-type orbitals[48]) [vs. N^7 for

full CCSD(T)[49]], a non-perturbative and multi-reference nature, and the ability to utilize a multiconfigurational SCF trial wavefunction. The ability to use a sophisticated multi-determinant trial is crucial for the treatment of many transition-metal-containing systems. Early AFQMC algorithms suffered from a very large prefactor, restricting applications to relatively small systems. Recent technical advances, including vastly improved efficiency for multideterminantal trial wavefunctions,[23,50] utilization of correlated sampling (CS) in the Monte Carlo protocol to directly compute energy differences,[51] and implementation on GPU hardware,[23,52] has made it feasible to treat significantly larger systems.[53–55]

These advances have allowed systematic studies of three classes of small transition metal containing species (atoms, diatomic molecules, and 4-6 coordinate complexes containing simple small molecule ligands) with highly encouraging results. Atomic ionization potentials,[23] diatomic bond energies,[29] and complex ligand dissociation energies,[54] have all been computed with a MAE of less than 1.5 kcal/mol across relatively large experimental gas phase data sets. These results outperformed both localized coupled cluster methods and the best DFT functionals. Furthermore, in all cases, the maximum outlier error was less than 3.5 kcal/mol, in contrast to alternative methods where errors in the 5-10 kcal/mol range were routinely observed.[54] Improved agreement with precise, state-of-the-art experimental data,[56] some of which were measured after the calculations were carried out, further validated the robustness of the AFQMC approach.

While the data sets enumerated above contained many very challenging electronic structure problems for which the accuracy of coupled cluster methods is expected to be lower than for organic molecules,[28,30,57] one could argue that the molecular structures that were studied are not representative of those considered relevant by inorganic chemists to biology, catalysis, and materials science. Firstly, the diatomic systems are small and coordinatively unsaturated. Secondly, the vast majority of cases involve low oxidation states of the metal which are rarely if ever seen in chemically relevant molecular species. The question then remains: can AFQMC deliver benchmark quality results for more prototypical larger and

more complex systems with typical (higher) metal oxidation states?

In the present paper, we study the adiabatic and vertical ionization energies of a series of six first row transition metal metallocenes, in which the metal (V through Ni) is in the II oxidation state, using AFQMC, DFT, and DLPNO-CCSD(T_0) methodologies. These systems are small enough to enable a large number of computational experiments to be carried out in order to explore which, if any, AFQMC protocols are necessary and sufficient to yield good agreement with experiment. They are also representative molecules for evaluating the expected performance for typical inorganic chemistry applications. Indeed, ferrocene oxidation is often used as a reference reaction in electrochemical measurement of redox potentials.[58] Finally, adiabatic gas phase experimental data, measured with electron transfer equilibrium (ETE) by Richardson and co-workers[59–61] with relatively low experimental uncertainties, as well as vertical gas phase experimental data, as measured with photoelectron spectroscopy by Green and co-workers,[45,62] exist for this series, which can form the basis to evaluate the accuracy of the various quantum chemical approaches for prototypical organometallic species, though this is not an exhaustive set. Metallocenes on their own are an important class of organometallic compounds, given their importance in alkene polymerization and electrochemistry.[63] Much of the previous literature of correlated calculations has focused on either predicting the spin splitting of metallocenes in solution,[64–66] which presents complications due to the solvent environment, and/or the bond dissociation energy of the M-Cp bond[67] rather than the ionization energy, which has a direct equivalent in solution and has both adiabatic and vertical variants. When the ionization energy is studied, it is usually just for ferrocene.[64,68]

A number of significant conclusions emerge from the metallocene calculations presented here. The localized coupled cluster approach that we have employed — DLPNO-CCSD(T_0) with the particular thresholds described in the methods section — displays a number of large outliers and an overall MAE that is comparable to those typically obtained from DFT functionals. To further probe the source of the errors, we have examined one of the more

challenging metallocene systems, $Mn(Cp)_2$, at higher levels of coupled cluster theory, tightening the cutoffs and replacing (T_0) with (T_1) in the DLPNO approach, and carrying out full CCSD(T) calculations in a small basis set. These calculations show considerable differences from our default DLPNO-CCSD(T_0) results, moving the computed ionization energies in the direction of the experimental value. Rigorously converging CCSD(T) (or even higher levels of excitation) to the CBS limit would be computationally very expensive, and hence is beyond the scope of the present paper. However, it is clear that further effort to test and develop scalable coupled cluster based methods for treating transition metal containing systems should be a high priority of the community, and is likely to yield fruitful results.

The gradient corrected, hybrid, and range-separated hybrid DFT functionals display MAEs between 3.5 and 5.5 kcal/mol for both the vertical and adiabatic ionization energies, with one or more individual errors greater than 7 kcal/mol; no functional performs at the lower end of this range for both data sets. The double hybrid functional DSD-PBEP86 displays significantly worse average errors and outliers than those seen in other functionals, in agreement with our prior results on other transition metal containing test sets, and consistent with discussions in the literature with regard to difficulties experienced by the current generation of these functionals for many transition metal containing systems.[69] Attempts to improve double hybrid performance for metal containing systems are at present ongoing in a number of research groups.

Motivated by these results, we also tested these DFT functionals and DLPNO-CCSD(T_0) on a second set of gas phase ionization energies measured by the same experimental group,[70,71] the tri-acetylacetonate (acac) systems (V through Co). These acac complexes are also an important set of coordination compounds with organic scaffolds, widely studied as models for other tris-β-diketonate complexes and as sources of transition metals in chemical vapor deposition processes.[71] Here, we find two molecules, namely $[Cr(acac)_3]^{1-}$ and $[Mn(acac)_3]^{1-}$, for which very large outliers are obtained, confirming the initial picture that one can often obtain quite accurate results, but that major failures can occur as well.

For the vertical and adiabatic metallocene ionization energies, we were able to develop a systematic AFQMC protocol that achieved accuracy within the experimental noise limitations. This was achieved by overcoming significant challenges arising from the greater size and complexity of the metallocene series (as compared to molecules in earlier publications).[23,29,54,55,72] For example, prior work[54] has demonstrated that it is essential to employ an appropriate multiconfigurational trial wavefunction, since calculations based on Hartree-Fock (HF) trial wavefunctions did not reliably lead to chemically accurate results for these systems. Deployment of an appropriate multiconfigurational trial wavefunction in the application of the AFQMC approach to transition metal containing systems remains essential if one is aiming at robust, benchmark quality results. Another key component of our protocol is to use correlated sampling (CS) to compute energy differences whenever the two (or more) systems can be effectively correlated. In this work all vertical ionization energies (including the vertical step of an adiabatic ionization) are computed by CS. We then validate geometry reorganization energies predicted by lower-level theories with separate AFQMC calculations using standard branching and population control (PC).

In the latter form of AFQMC calculations, MC sampling is carried out independently for two different states and, at intervals, walkers with large weights are duplicated while those with small weights are destroyed with appropriate probability via a "comb" algorithm.[48] This is needed to mitigate the weight fluctuations in the branching random walk to maintain Monte Carlo sampling efficiency. A CS simulation typically can be carried out for a much shorter duration, during which the need for PC of AFQMC walkers is minimized and the accruement of phaseless constraint error is sometimes reduced. How robust this type of behavior is when considering a wider class of systems remains an open question worthy of more systematic future investigation.

We have shown in previous work that the use of CS is highly effective in obtaining accurate energy differences between different electronic surfaces for a number of very challenging cases, and can in fact produce more accurate results than pure PC in some cases.[29,54] The use of

CS AFQMC to measure energy differences for vertical transitions, and PC AFQMC, rather than DFT, to measure differences between two geometries on the same surface appears to be a very promising approach for all cases in this work. Of course, considerable additional comparison with experiment will be required in order to rigorously assess errors across a wide range of relevant transition metal containing systems.

This paper is organized as follows. In Section II, we discuss the experimental data for the metallocene and acac series that we will be focusing on in our computational work. In Section III, we briefly review the AFQMC methodology and the previous results obtained using it, and describe the DLPNO-CCSD(T_0) and DFT methods employed. Section IV presents results of AFQMC, various DFT functionals, and DLPNO-CCSD(T_0) calculations for the metallocene series, as well as DFT and DLPNO-CCSD(T_0) results for the acac series, which will be studied by AFQMC in future work. We also show that using experimentally derived solvation free energies in concert with accurate gas-phase predictions leads to accurate solution-phase reduction potentials. In Section V, we consider the implications of our results for the utility of DFT, DLPNO-CCSD(T_0), and AFQMC in addressing transition metal chemistry. Finally, in Section VI we conclude with a summary of our results and outline future directions.

II. Experimental Data Sets

The gas-phase ionization energy experiments that we investigate below center on first row transition metals in the II or III oxidation state, with either anionic cyclopentadienyl (Cp) ligands (metallocenes) or acetylacetonate ligands (acac series), depicted schematically in Figs. 1a and 1b, respectively.

The metallocenes we investigate are vanadocene, chromacene, manganocene, ferrocene, cobaltocene, and nickelocene. The ionization processes we study are for the II oxidation state (charge = 0) to the III oxidation state (charge = +1). All of the metallocene molecules in

these two oxidation states are low spin complexes, except for Mn(II), which is a sextet, and Mn(III), which is a quintet for the vertical experiments (as discussed below). The acac species in the II oxidation state (charge = -1) are ionized to form the III oxidation state (charge = 0). Note that in the original work by Richardson and co-workers, what is actually reported is the "attachment" energy,[70,71] meaning the reduction energy from oxidation states III to II, but we reverse the sign here to facilitate comparison to the ionization of metallocenes. All of the acac molecules in these two oxidation states are high spin complexes, except for Co(III) which is a singlet. The ground state multiplicities/term symbols of all species are given in Table 1.[41,60–62,62,67,73,73–78] The expected ground state term symbols from the acac complexes come from standard Tanabe–Sugano diagrams; we do not explicitly constrain the geometric symmetry or term symbols of our calculations, merely the multiplicity and charge.

Table 1: The expected ground state term symbols of the metallocene or acac complexes in III or II oxidation states.

Oxidation State	III	II	III	II
Ligand	Cp	Cp	acac	acac
Metal				
V	$^3A_2$	$^4A_2$	$^3T_1$	$^4A_2$
Cr	$^4A_2$	$^3E_2$	$^4A_2$	^5E
Mn	$^3E_2$ ($^5E_1$)	$^6A_1$	^5E	$^6A_1$
Fe	$^2E_2$	$^1A_1$	$^6A_1$	$^5T_2$
Co	$^1A_1$	$^2E_1$	$^1A_1$	$^4T_1$
Ni	$^2E_1$	$^3A_2$	-	-

The adiabatic experimental values come from the electron transfer equilibrium (ETE) measurements of Richardson and co-workers.[59–61] These experiments utilize Fourier transform ion cyclotron resonance mass spectrometry (FTICR-MS) to determine adiabatic ionization energetics for organic and inorganic species near room temperature. From the measured equilibrium constants for the electron-transfer reactions, the free energies of reaction are determined, and from this information the free energies of ionization can be inferred. The energies in solution are obtained using the solution phase potentials and the 4.44 V abso-

lute potential of the standard hydrogen electrode (SHE) in water at 298.15 K, derived using various thermodynamic quantities, such as the solvation energy of a proton.[79] Because these experiments were performed at 350 K, we use this temperature value in our calculated free energy corrections.

(a) Metallocene compounds (M = V to Ni). (b) acac compounds (M = V to Co).

Figure 1: The structure of the metal complexes studied.

The vertical experimental values come from the photoelectron spectroscopy (PES) measurements of Green et al.,[45,62] who used UV and X-ray photons to ionize samples via the photoelectric effect and measure the kinetic energy (KE) of the ejected photon with a frequency ν. The binding energy (BE) is then determined by the equation $BE = h\nu - KE$, where h is Planck's constant.

III. Computational Details

The geometries, certain reorganization energies (*vide infra*), and ideal gas free energy corrections[80] were obtained with the B3LYP functional[5–7] utilizing the cc-pVTZ-DKH[81–84] basis set and DKH2 relativistic corrections[85] using the one-center approximation (as implemented in ORCA) and without symmetry constraints. Geometries were confirmed to be minima using normal-mode analysis. These calculations were performed using the ORCA program package.[86] In the cc-pVTZ-DKH basis set, metallocenes typically have around 508 basis functions and 95 electrons. In the same basis set, the acac complexes are roughly twice as large from an electronic structure perspective with 992 basis functions and 183 electrons.

Information regarding integration grids and other theoretical details can be found in the SI.

We investigated the addition of D4[87] dispersion to the geometry optimization of $MnCp_2$. Consistent with previous results,[67] we find the geometry is relatively similar to that without these dispersion corrections, as discussed in the SI. We also have evaluated the B3LYP-D4 energetics for the ionization energies of both the metallocenes and acac complexes and find similar results to those found below, as discussed in the SI.

Utilizing diffuse functions in the basis set for both metallocenes (aug-cc-pVTZ on all atoms) and acac complexes (aug-cc-pVTZ on the O atoms), which one might argue could be significant because of the anionic ligands, yields very similar results, as is discussed in the SI. Similar calculations for the metallocenes, but with the diffuse functions on the C using B3LYP yield similar MAE's.

Unrestricted DLPNO-CCSD(T_0) (T_0 refers to the semi-canonical approximation to the perturbative triples correction[18]) calculations were performed with quasi-restricted orbitals (QROs) generated from unrestricted B3LYP reference orbitals and "NormalPNO" (moderate energy cutoff criteria for correlation between localized orbitals) localization parameters using ORCA. These calculations utilized cc-pVxZ-DKH and auxiliary cc-pVxZ\C basis sets, where x is the cardinal number of the basis set (i.e. x=3,4 for TZ,QZ), as built into ORCA,[86] as discussed in the SI. TZ/QZ extrapolation schemes have been used successfully for AFQMC.[23,29,51,54,72,88] Such extrapolation (typically with TZ/QZ basis sets) or at least evaluation at QZ has been shown to be important in various applications of DLPNO-CCSD(T).[20,89–93] We extrapolate to the complete basis set (CBS) limit for absolute energies using exponential and $\frac{1}{x^3}$ dependence for the HF and correlation energies, respectively,[94] The keyword "NoFrozenCore" was used so that no electrons would be frozen. The SI shows that not including this keyword would not significantly change the results. For these calculations, the one-center approximation was not used for the relativistic corrections.

As discussed in the SI, we investigated the convergence of the DLPNO-CCSD(T_0) results with respect to the PNO cut-off values, including extrapolating the TCutPNO parameter to

0,[93] and the treatment of the (T) for the case of $MnCp_2$, which turns out to be the biggest outlier for DLPNO-CCSD(T_0) for our adiabatic results discussed below. We also compare to full CCSD(T) in the DZ basis set. The results do improve significantly (from an error of about 10 kcal/mol to about 1.5 kcal/mol from experiment) with the use of increasingly tight PNO cut-off criteria and iterative T_1 corrections. Preliminary results suggest that the CBS limit would not be much different. Such an error reduction is beyond the errors seen from the use of NormalPNO by others.[20,92,95] Nevertheless, we limit our interpretation of the coupled cluster results to the version of DLPNO-CCSD(T_0) that we used and propose that further investigation of these systems with coupled cluster variants is warranted, given the expense of running the most rigorous implementation.

Electron repulsion integrals and the Hamiltonian for ph-AFQMC were obtained with PySCF.[96] The exact-two-component (x2c) relativistic Hamiltonian[97] was used in place of DKH2, as the latter is not implemented in PySCF.

While ph-AFQMC can be extended to excited states,[98] the implementation we use is limited to studying the ground state of a given combination of charge, multiplicity, and geometry. The ph-AFQMC propagation utilized an imaginary time step of 0.005 E_h^{-1} (these units are also referred to Ha^{-1} or β in the literature), which in our experience is sufficiently small in these systems such that errors from the Trotter decomposition are negligible given our target statistical accuracy.[51] We utilize single precision (sp) rather than double precision (dp) floating point arithmetic, as discussed in the SI. Walkers were either initialized with a RHF/ROHF determinant or according to a distribution of CASSCF determinants weighted by their respective CI coefficients. Initialization with restricted orbitals ensures spin-purity, even in the case of a UHF trial wavefunction.[99] Additional details are given in the SI.

For the main ph-AFQMC computations using the cc-pVTZ-DKH basis set, we utilized CASSCF trial wavefunctions. The default active space for generating the trial wavefunction was automatically determined via the atomic valence active space (AVAS) procedure, where only those orbitals that overlap significantly ($\sim 10\%$) with the 3d and 4d orbitals (as

defined from the Atomic Natural Orbital (ANO-RCC) basis set)[100] of the metal ion were included.[101] This active space thus targets the static correlation of the metal rather than the ligands. These active spaces were typically around 14 electrons in 15 orbitals. We typical retain 98% of the CI weight (the minimum was 96%), resulting in about 300 determinants. RCAS/AFQMC calculations were determined to be converged with respect to the active space size by testing active spaces of increasing size until the resulting calculations were equivalent within statistical accuracy. If the natural orbital occupation numbers (NOONs) resulting from this approach were not physical (e.g. the fractional change in occupation in the occupied orbitals is not reflected in the virtual orbitals), alternate active spaces were selected using other approaches, such as using the frontier orbitals without modification, or using the MINAO basis set with 3d and/or $2p_z$ orbitals, as described in the SI.

The CBS limit for the ph-AFQMC calculations was estimated using an approach similar to that described in previous work.[54] Briefly, we extrapolate the ionization energy computed with ph-AFQMC PC with the cc-pVxZ-dkh basis sets (x=3,4 for T,Q) using an inexpensive trial wavefunction such as UHF or a CASSCF wavefunction with a small active space. The UHF ionization energy is extrapolated using an exponential form. The contribution to the ionization energy from the correlation energy computed by AFQMC is extrapolated using a $1/x^3$ functional form. This method is equivalent to fitting the procedure discussed above for the CBS extrapolation of DLPNO-CCSD(T_0), though there we extrapolate the *absolute* rather than the *relative* energy. This "low-level" result is used, in turn, to extrapolate the "high-level" ionization energy computed with a large CAS trial in the x=3 basis. A scaling factor, ρ the ratio of the correlation energies between low and high levels of AFQMC is used to translate the basis dependence of the least sophisticated trial to a result that approximates one with a better trial function,

$$\rho = \frac{\Delta E^{corr}(\text{TZ, high-level})}{\Delta E^{corr}(\text{TZ, low-level})}. \tag{1}$$

Whether or not a CAS trial is used for the extrapolation is determined by identifying which cases appear to exhibit significant multireference character, as can be flagged by deviations of the CASSCF NOONs and $\langle S^2 \rangle_{B3LYP}$ from ideal values.

Our CS approach[51] enables fast convergence of vertical energy differences between similar states of a system, e.g. reduced/oxidized states, by employing a shared set of auxiliary fields, effectively leading to a cancellation of statistical error and, in many cases, also fast (quasi-)equilibration. The absence of PC results in CS requiring more initial walkers, but the reduced statistical fluctuations from correlated samples allow for a much shorter propagation time. Empirically, we find that 15 E_h^{-1} allows full equilibration of the accuracy differences while providing excellent statistical accuracy. For this approach to be justified, it is necessary that the simulations produce a "quasi-plateau" in the targeted energy difference for relatively short imaginary times which better approximates the unbiased result. In the cases we have investigated, we *empirically* note such a stable regime in imaginary time. Cross checks with the corresponding independent AFQMC runs can help to validate convergence.

CS has been shown to improve the accuracy of the calculated energy differences in certain situations, due to correlated and faster convergence of the energy differences, which avoids the full onset of the phaseless constraint error.[23,29,54] For $MnCp_2$, we also checked that the use of an alternate, more rigorous approach to CS produces the same ionization energy as the original algorithm (details provided in the SI, and in a future publication). Results across three different types of data sets[29,51,54] suggest that the CS methodology achieves a greater reliability than PC approaches in comparing different electronic surfaces to within near chemical accuracy.

Since CS calculations are most effective if the geometry of the two surfaces is held constant, the ionization energy (IE), is computed by

$$IE = G(III) - G(II) - \lambda, \tag{2}$$

where G is the free energy obtained by correcting the electronic energy with terms that account for temperature effects. The reorganization energy, λ, is defined as the difference in energy between the III product in its optimal geometry and in the II reactant geometry. λ is computed via either B3LYP/cc-pVTZ-DKH, as in our previous work,[54] or the PC ph-AFQMC with either a UHF or CAS trial wavefunction, as described in the Results section. The approximation of using B3LYP for the reorganization produces very poor results for one case (manganocene), as we will discuss further below, as there is a large change in equilibrium geometry between the II and III states. Evaluating the reorganization energy with AFQMC calculations for the two geometries remedies this problem, and yields highly satisfactory agreement with experiment for all cases. The calculation of IEs is illustrated in Fig. 2.

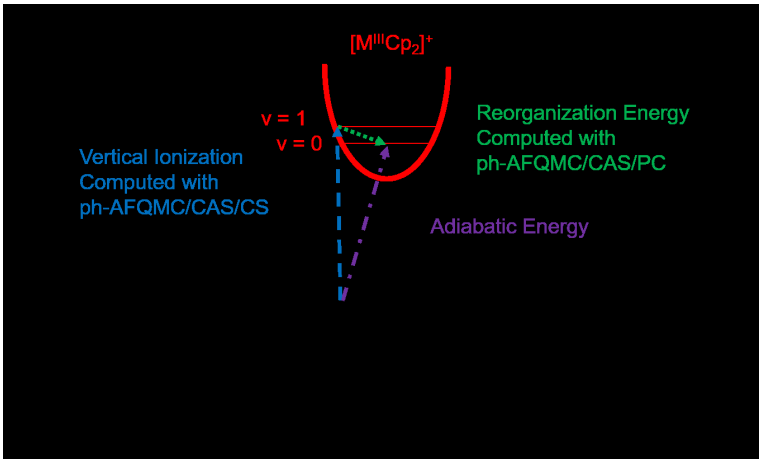

Figure 2: Schematic of the ionization and reorganization energy calculations performed in this work. CS and PC indicate the energy was measured by the CS and PC approaches, respectively. The v labels for vibrational energy levels are arbitrary.

For our CS calculations, we typically ran 30 repeats, with 6624 walkers ($\simeq$ 200,000 walkers in total) and 276 GPUs (46 nodes) each until 15 E_h^{-1}. For our PC calculations, we typically ran for 2000 E_h^{-1} (or shorter for QZ calculations) using 3312 walkers and 552 GPUs (92 nodes). To give a sense of the required computational cost, a CS ph-AFQMC calculation for $[Mn^{III}Cp_2]^0$ requires about 1,231 node hours on Summit ($<$ 1 hour walltime), using a truncated (99.5% of the weight) CASSCF trial wave function containing 282 determinants.

These settings typically allowed us to obtain statistical error bars in the energy difference below 2 kcal/mol.

We compare ph-AFQMC with the local GGA BP86,[102,103] hybrids B3LYP,[5] B3LYP*,[104] PBE0,[10] and B97,[8,9] the meta-GGA hybrids M06[105] and TPSSh,[106,107] the semilocal meta-GGA (non-hybrid) B97M-V,[108] the range-separated hybrid meta-GGA ωB97M-V,[109] the range-separated hybrid ωB97X-V functionals,[110] and the double-hybrid DSD-PBEB86.[111,112] These calculations were done in ORCA. We perform single-point energy calculations, without the one-center approximation for the relativistic corrections. The MP2 part of the double-hybrid calculations used the frozen core approximation (10 electrons ($1s^2 2s^2 2p^6$) for 3d transition metals and 2 electrons for C and O ($1s^2$)). B3LYP geometries were obtained using the large "Grid7" option in ORCA (see SI).

IV. Results

Vertical Ionization Energies

The vertical IE results using ph-AFQMC methods are given in Table 2. AFQMC PC/UHF has numerous large outlier cases, such as $CrCp_2$ and $NiCp_2$. Both AFQMC PC and AFQMC CS with CAS trials are significant improvements over AFQMC PC/UHF. The CS results have a lower maximum error. The PC results show a greater dependence on the quality of the trial wavefunction.

The CASSCF NOONs of both ^{5}Mn(III) and Ni(III) show a small but notable fractional occupation of the lowest unoccupied natural orbital (LUNO) of at least +0.165, which can be traced to a loss of occupation of at least -0.16 in one of the occupied orbitals. In both cases, these deviations from ideal NOONs are accompanied by a deviation of $\langle S^2 \rangle_{B3LYP}$ from the expected value. The Mn and Ni cases deviate from the ideal values by 5.54% and 6.38%, respectively. Non-integer CASSCF NOONs and spin-symmetry breaking in unrestricted DFT calculations have been put forth as complementary diagnostics of static correlation in tran-

sition metal compounds, as they reflect a wavefunction that is a superposition of more than one spin state made possible by a near-degeneracy of energy levels.[69] Indeed, the calculated M-Cp lengths (Table S29) and experimental gas-phase homolytic M-Cp dissociation energies (Table S30)[60,61] together imply that bonding is weakest in the Mn and Ni complexes across the 3d series. In general, as the strength of a bond weakens, the energy splitting between spin states narrows, setting the stage for static correlation. While most simply illustrated when diatomics such as H_2 or N_2 are stretched, an analogous situation has previously been reported for a weakly bound tetraammine Mn cation in the gas phase.[69] While the degree of multireference character implied by these methods can be sensitive to the active space and DFT functional employed, respectively, we propose (and certainly find in this dataset) that this procedure has utility for pinpointing particularly difficult cases, independent from any comparison to experiment.

Due to the presence of particularly extensive correlation in the Mn and Ni cases, we apply an improved extrapolation, using AFQMC PC/CAS rather than with AFQMC PC/UHF. We used AVAS and the MINAO basis set to generate active spaces of 8-10 electrons in 8-10 orbitals for $Mn^{II}Cp_2$, $^5Mn^{III}Cp_2$, and all three $NiCp_2$ species in both TZ and QZ basis sets for use in AFQMC. Using these trial wavefunctions instead of the UHF trial wavefunctions to extrapolate the vertical AFQMC CS/CAS value resulted in a value of 153.14 ± 1.72 kcal/mol for the Mn case, which agrees reasonably well with the experimental value of 150.1 ± 2.31 kcal/mol, considering the uncertainties in both values. The value with a UHF trial extrapolation is 157.08 ± 1.72 kcal/mol, which is clearly in worse agreement with experiment and outside of the joint error bars of theory and experiment. The Ni case was also significantly improved. Finally, as a control, we ran calculations using the CASSCF-trial CBS extrapolation for $CoCp_2$, which did not require it according to our criteria, and obtained very similar results to those found with the use of the UHF trial (see SI).

The accuracy of these vertical excitation results implies that, coupled with accurate calculation of the reorganization energy, we should find accurate adiabatic results. Indeed,

the photoelectron spectroscopy results may be more difficult to interpret than the adiabatic experiments, due to a variety of factors. For example, we do not attempt to compute vibronic contributions or to include temperature effects. Additionally, the vertical experiments exhibit an increased uncertainty due to the difficulty in interpreting the spectra in terms of line width. Moreover, the "excited" vertically ionized state, in a distorted, nonequilibrium geometry, is naturally harder for electronic structure methods to compute as compared to the equilibrium geometry of the ground state.

Table 2: Vertical ionization energies as a function of metallocene type and AFQMC methodology. The mean absolute errors (MAE), maximum errors (MaxE), root-mean-square deviations (RMSD), and the mean signed errors (MSE) are included. All units are in kcal/mol.

	PES Expt	AFQMC PC/UHF	AFQMC PC/CAS	AFQMC CS/CAS
$V(Cp)_2$	156.3 ± 2.31	158.95 ± 1.59	161.4 ± 2.16	155.34 ± 1.51
$Cr(Cp)_2$	131.4 ± 2.31	123.49 ± 1.31	129.29 ± 1.86	127.27 ± 1.85
$Mn(Cp)_2$	159.3 ± 2.31	159.29 ± 0.72	158.51 ± 1.00	156.56 ± 0.78
$Fe(Cp)_2$	158.7 ± 2.31	161.09 ± 1.92	161.1 ± 2.3	155.38 ± 1.88
$Co(Cp)_2$	128 ± 2.31	126.23 ± 1.87	127.5 ± 1.89	129.22 ± 1.44
$Ni(Cp)_2$	150.1 ± 2.31	157.89 ± 1.33	153.19 ± 0.97	153.14 ± 1.72
MAE		3.75 ± 1.13	2.33 ± 1.13	2.57 ± 1.13
$\|MaxE\|$		7.91 ± 1.13	5.1 ± 1.13	4.13 ± 1.13
RMSD		4.82	2.79	2.81
MSE		0.53 ± 1.13	1.2 ± 1.13	-1.15 ± 1.13

The DFT and DLPNO-CCSD(T_0) results for vertical ionization energies, using the various functionals enumerated in section III are compared to ph-AFQMC in Fig. 3 and are enumerated in Table 3.

The hybrid functionals B3LYP B3LYP*, M06, B97, PBE0, TPSSh, ωB97X-V and ωB97M-V, as well as the meta-GGA B97M-V all have MAE's between 4.5 and 5.7 kcal/mol indicating similar performance, given the uncertainty of the experiments. The double hybrid functional DSD-PBEP86 also does not perform very well, especially for $CoCp_2$, which may be due to the difficulty that MP2-based methods have for organometallic complexes, as discussed in Ref. 69. The lower RMSD observed for the BP86 functional must be considered fortuitous in

view of the very large errors obtained for the adiabatic calculations in Table 6 below. Among different functionals, the maximum error often occurs at different metallocenes, indicating a lack of predictable reliability.

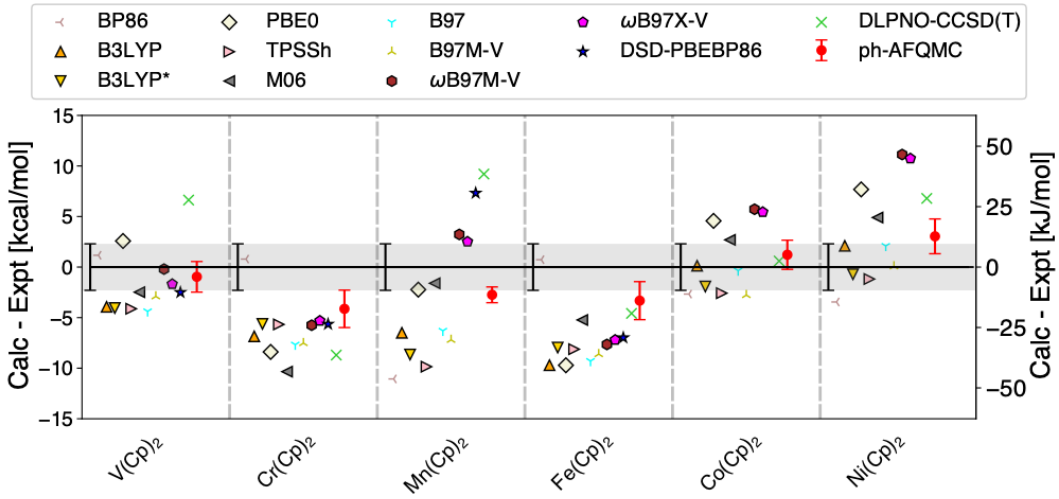

Figure 3: Performance of ph-AFQMC (CAS trial, CS), DFT functionals (QZ basis), DLPNO-CCSD(T_0) (extrapolated with TZ/QZ basis sets), and experiment for prediction of experimental vertical gas-phase ionization energies for metallocenes. The range is limited to deviations of -15 to 15 kcal/mol. The DSD-PBEP86 result for $Co(Cp)_2$ and $Ni(Cp)_2$ are out of range with deviations of about -20 and 17 kcal/mol respectively. The gray band indicates the uncertainty of the experiments i.e. 2.31 kcal/mol.

Table 3: DFT (QZ basis) and DLPNO-CCSD(T_0) (extrapolated with TZ/QZ basis sets) vertical ionization energies, as a function of metallocene and methodology. The mean absolute errors (MAE), maximum errors (MaxE), root-mean-square deviations (RMSD), and the mean signed errors (MSE) are included. All units are in kcal/mol.

	Expt.	BP86	B3LYP	B3LYP*	PBE0	TPSSh	M06	B97	B97M-V	ωB97X-V	ωB97M-V	DSD-PBEP86	DLPNO-CCSD(T)
$V(Cp)_2$	156.3 ± 2.3	157.47	152.37	152.25	158.88	152.18	153.82	151.92	153.40	154.62	156.10	153.80	162.93
$Cr(Cp)_2$	131.4 ± 2.3	132.19	124.55	125.78	123.01	125.73	121.06	123.73	123.88	126.09	125.65	125.76	122.70
$Mn(Cp)_2$	159.3 ± 2.3	148.24	152.80	150.65	157.07	149.45	157.70	153.00	152.10	161.81	162.53	166.62	168.50
$Fe(Cp)_2$	158.7 ± 2.3	159.43	149.00	150.74	148.99	150.58	153.47	149.41	150.09	151.50	151.05	151.72	154.12
$Co(Cp)_2$	128 ± 2.3	125.33	128.13	126.08	132.57	125.42	130.69	127.65	125.23	133.44	133.72	108.35	128.60
$Ni(Cp)_2$	150.1 ± 2.3	146.65	152.20	149.39	157.78	148.92	155.00	152.19	150.17	160.84	161.23	167.29	156.89
MAE		3.31	4.87	4.82	5.86	5.25	4.54	5.01	4.84	5.48	5.61	9.88	6.08
$\|MaxE\|$		11.06	9.70	8.65	9.71	9.85	10.34	9.29	8.61	10.74	11.13	19.65	9.20
RMSD		4.90	5.82	5.63	6.53	6.05	5.39	5.89	5.75	6.25	6.57	11.70	6.73
MSE		-2.42	-4.12	-4.82	-0.92	-5.25	-2.01	-4.32	-4.82	0.75	1.08	-1.71	1.66

Reorganization Energies

Table 4 gives the reorganization energies along the III potential energy surface (except for $MnCp_2$ where we use the low spin surface) for the various metallocenes using B3LYP AFQMC with PC and a UHF trial (AFQMC PC/UHF), and AFQMC with PC and a CAS trial (AFQMC PC/CAS). We see that B3LYP reorganization energies are outside AFQMC error bars in all cases. The reorganization energies are fairly similar for VCp_2, $CrCp_2$, and $FeCp_2$. The AFQMC results disagree with B3LYP for $CoCp_2$ and the AFQMC/CAS result shows significant differences the other two for $NiCp_2$.

The discrepancy between all methods is very large for $MnCp_2$. The reorganization energy for the Mn system is expected to be large given the large geometry change in going from II to III.[61] In particular, the B3LYP M-Cp ring centroid distance decreased from 2.08 Å to 1.78 Å. To explore this further, we systematically changed the Mn^{III}-Cp centroid distance and calculated the energy along this coordinate (optimizing other degrees of freedom) using B3LYP and AFQMC/UHF. Fig 4 shows that the equilibrium position from both methods are similar, but at higher distances, where the Mn^{II} geometry would be found, the PES curves differ significantly, with the AFQMC/UHF curve well above the B3LYP curve, indicating its reorganization energy will be higher, as we observe. We use different AFQMC reorganization energies to calculate adiabatic ionization energies and compare the results to experiment in the next section.

Table 4: Reorganization energies calculated in the TZ basis along the III potential energy surface as a function of metallocene and methodology. All units are in kcal/mol.

	B3LYP	AFQMC PC/UHF	AFQMC PC/CAS
$V(Cp)_2$	0.37	1.73 ± 0.58	1.76 ± 0.52
$Cr(Cp)_2$	3.04	0.14 ± 0.5	-0.19 ± 0.52
$Mn(Cp)_2$	28.46	52.38 ± 0.7	41.5 ± 0.68
$Fe(Cp)_2$	3.17	0.82 ± 0.71	0.87 ± 0.69
$Co(Cp)_2$	6.57	12.45 ± 0.79	10.75 ± 0.66
$Ni(Cp)_2$	6.30	11.34 ± 0.72	11.04 ± 0.57

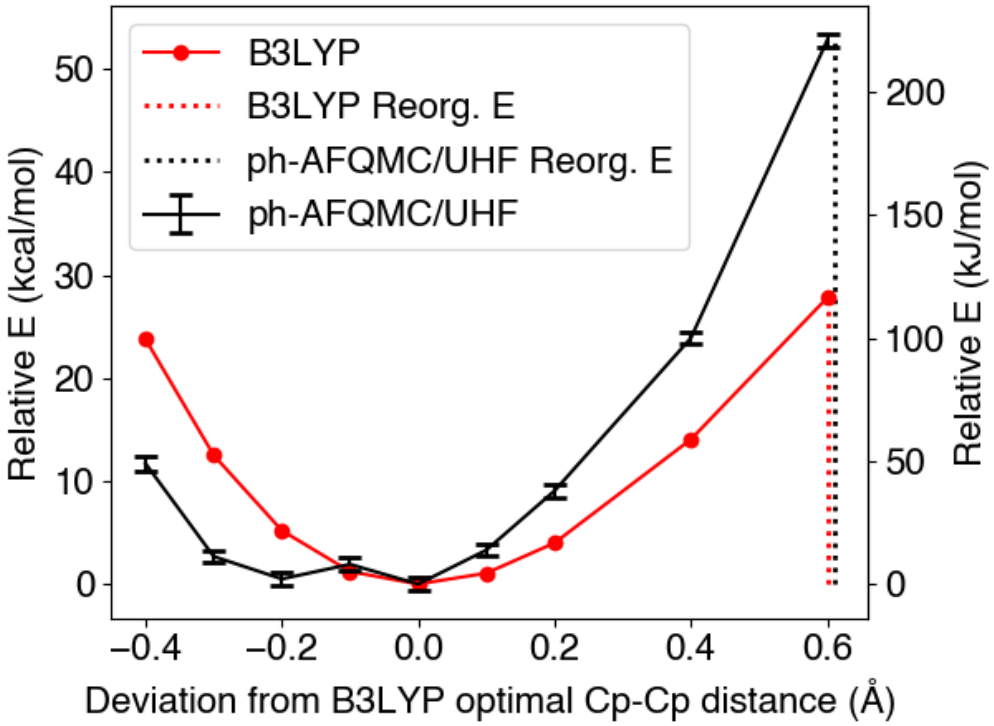

Figure 4: Rigid scans of the Cp-Cp distance in $[Mn^{III}Cp_2]^{1+}$ where red = B3LYP and black = ph-AFQMC/UHF. The x-axis is the deviation from the B3LYP optimal Cp to Cp ring distance of 3.55 Å. The dashed vertical lines indicate what the reorganization energy would be at the optimal ring distance of $[Mn^{II}Cp_2]^0$.

Adiabatic Ionization Energies

The adiabatic ionization energies using different AFQMC methods are compared to experiment in Table 5. With AFQMC CS, the adiabatic ionization energy is computed with the two-step procedure illustrated in Fig. 2, while with AFQMC PC, it is computed directly as a two-point energy difference (purple line). AFQMC using PC with either a UHF trial or a CAS trial does not perform well, with similar MAE's, absolute maximum errors, and other statistical measures. Much of the poor performance is for $MnCp_2$. The poor performance of AFQMC using PC is likely due to an inferior trial wavefunction, which is perhaps not converged with respect to active space, particularly for the III oxidation state, and potentially poor error cancellation. The results using AFQMC with CS, CAS trial, and B3LYP

reorganization energies, called AFQMC CS (1), performs similarly poorly due to this outlier. However, using AFQMC-generated reorganization energies results in much better agreement with experiment. We interpret this success as follows: The vertical excitation from the II to the III state has the largest change in electronic structure and hence is most demanding; CS succeeds because the energy difference can be converged before the full bias due to the phaseless constraint appears, and exploits cancellation of error in the Monte Carlo sampling on the II and III surfaces. For the reorganization energy, DFT methods appear to have difficulty obtaining accurate results for these transition metal containing systems at geometries that are substantially distorted from the minimum; AFQMC/PC provides accurate results for such distortions, at least for the present systems.

Table 5: ph-AFQMC adiabatic ionization energies at the complete basis set limit as a function of metallocene and methodology. The mean absolute errors (MAE), maximum errors (MaxE), root-mean-square deviations (RMSD), and the mean signed errors (MSE) are included. All units are in kcal/mol. (1) = B3LYP reorganization energy and (2) = AFQMC PC/CAS reorganization energy. All units are in kcal/mol.

	ETE Expt	AFQMC PC UHF Trial	AFQMC PC CAS Trial	AFQMC CS (1) CAS Trial	AFQMC CS (2) CAS Trial
$V(Cp)_2$	154.5 ± 1.5	157.64 ± 1.55	160.25 ± 2.15	155.44 ± 1.61	153.7 ± 1.52
$Cr(Cp)_2$	127.5 ± 1.5	127.04 ± 1.43	133.54 ± 1.96	127.63 ± 1.81	131.18 ± 2
$Mn(Cp)_2$	142.5 ± 1.5	156.26 ± 1.54	151.69 ± 2	158.53 ± 1.97	146.09 ± 2.37
$Fe(Cp)_2$	153.1 ± 1.5	158.41 ± 1.84	158.37 ± 2.32	150.34 ± 1.75	152.78 ± 2.02
$Co(Cp)_2$	123.5 ± 1.5	119.06 ± 1.6	122.18 ± 1.85	128.1 ± 1.52	124.35 ± 1.83
$Ni(Cp)_2$	143.8 ± 1.5	144.75 ± 1.42	143.49 ± 1.64	148.25 ± 1.7	144.25 ± 2.15
MAE		4.68 ± 0.89	4.65 ± 1.02	4.82 ± 0.93	1.61 ± 1.02
$\|MaxE\|$		13.76 ± 2.15	9.19 ± 2.5	16.03 ± 2.47	3.68 ± 2.5
RMSD		6.43	5.53	7.15	2.16
MSE		3.04 ± 0.89	4.1 ± 1.02	3.9 ± 0.93	1.24 ± 1.02

DFT results for the metallocenes using a variety of functionals are given in Table 6 using the QZ basis set, as is recommended in Ref. 113. DLPNO-CCSD(T_0) results are also given. The MAEs, and average errors, of all of these methods (other than the double hybrid functional DSD-PB86, which again displays the worst performance) are in a range similar to that observed for the vertical ionization energies, between 3.5 and 5.5 kcal/mol, with a maximum error greater than 7 kcal/mol. None of these results are overall of benchmark

quality, although the best performing functionals do obtain good results for individual cases. This data can be contrasted with the significantly lower MAE and maximum error obtained from the best AFQMC protocol. In fact, the performance is consistent with the prior results that we have reported for transition metal diatomics (bond dissociation energies)[29] and small coordination complexes (ligand removal energies).[54] The best methods are in the ballpark for many cases, but predictions are lacking in robustness.

An important question to ask at this point with regard to the DLPNO-CCSD(T_0) results is to what extent the errors are due to the specific approximations (both localized orbital cutoffs and the use of the less rigorous (T_0) representation of triple excitations), as opposed to an intrinsic limitation of CCSD(T) itself. This is a challenging issue to explore, because the use of more computationally expensive approximations becomes problematic for systems as large as the metallocenes (let alone grand challenge problems in biology and materials science, such as the water splitting cluster in Photosystem II). Nevertheless, we have made an initial effort to address this issue, varying the localization cutoffs and triples implementation (replacing T_0 with T_1) as detailed in the SI, for the $Mn(Cp)_2$ system. The use of tight cutoffs and T_1 brings the results to within 3-4 kcal/mol of experiment; using a DZ basis set to evaluate full CCSD(T) (all that we could afford) and extrapolating with DLPNO results, one would appear to come quite close to experiment (although one would have to be concerned about the accuracy of this protocol, given the large differences between the various coupled cluster approaches).

To provide a further assessment of preliminary DFT and DLPNO-CCSD(T_0) (using our default cutoff settings), we decided to carry out calculations for the acac series of coordination complexes described above. These systems have nearly double the number of electrons as the metallocenes, which presented difficulties with regard to obtaining results using our current AFQMC code. We have recently made major improvements to the code's performance and scaling with system size, and so it is likely we will be able to report converged results for the acac series in the near future. Results for our entire suite of DFT functionals, along

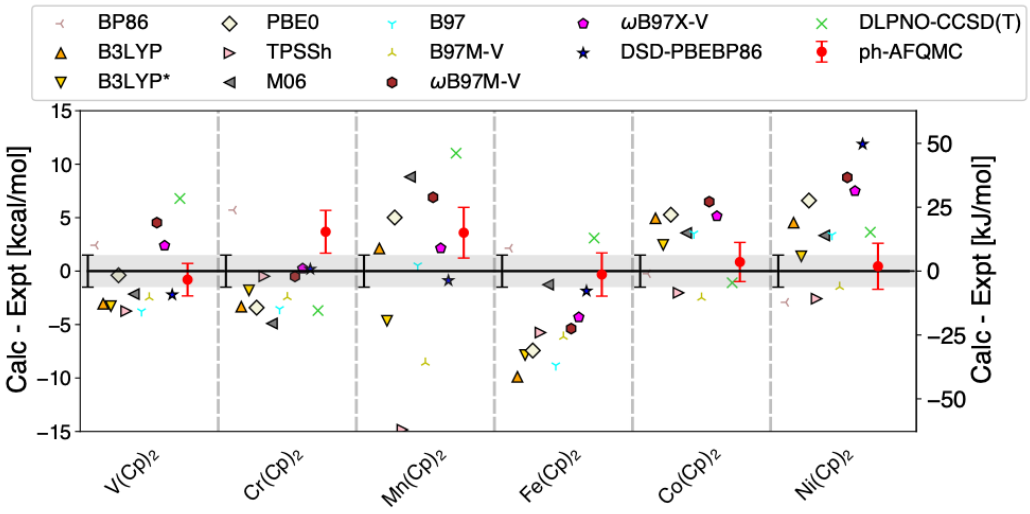

Figure 5: Performance of ph-AFQMC, DFT functionals (QZ basis), and DLPNO-CCSD(T_0) (extrapolated with TZ/QZ basis sets) for prediction of experimental adiabatic gas-phase ionization energies for metallocenes. The range is limited to deviations of -15 to 15 kcal/mol. The BP86 value for $Mn(Cp)_2$ and the DSD-PBEP86 value for $Co(Cp)_2$ are beyond of the range of the plot with deviations of about -20 and -25 kcal/mol, respectively. The gray band indicates the uncertainty of the experiments i.e. 1.5 kcal/mol.

with those for DLPNO-CCSD(T_0), are presented in Table 7 and Fig. 6 below. In what follows, we focus attention on adiabatic ionization potentials, as we have not evaluated vertical ionization energies for the acac series. We use the same QZ basis as was employed in studying the metallocenes.

A number of striking features of the data are immediately apparent. Firstly, none of the DFT methods perform as well as the best performers do for the metallocene series; the MAE and RMSD are in all cases well above (near-)chemical accuracy. This performance may in part be due to the net negative charge residing on the molecule, which can delocalize onto the metal in the III state, resulting in overbinding (as has been observed in organic systems). It should also be noted that the two acac cases with anomalously large errors (Cr and Mn) are the only ones which involve ionization from singly occupied e_g orbitals. Previous work has shown that the errors in removing or adding electrons to DFT orbitals depends significantly upon whether the orbital is singly or doubly occupied, and what type of orbital is involved.[41,42,114]

The B97, B3LYP, and ωB97M-V functionals yield the best results, at 4.56, 4.82, 4.94 kcal/mol MAE respectively, but it must be noted that ωB97M-V was one of the worst performing functionals for the metallocenes, with an MAE of 5.43 kcal/mol. Interestingly the performance of the double hybrid functional DSD-PBEP86 is relatively similar between metallocenes and acac complexes. Across both data sets, all of the DFT functionals exhibit several failures with quite large errors. Secondly, the DLPNO-CCSD(T_0) results are no better than the DFT results for, e.g., the range-separated hybrids. Thirdly, some of the DFT error appears to be systematic in character, with similar trends being manifested for many of the DFT functionals. A particularly extreme example can be found for the $[Cr(acac)_3]^{1-}$ species, for which most of the DFT functionals yield an adiabatic ionization potential that is $\sim$10 kcal/mol smaller than experiment. Assuming that the acac experiments have error bars that are similar to those of the metallocene experiments (the latter having been validated by the close agreement of the experimental data with the AFQMC results), we can conclude from the above results that both DFT and the version of DLPNO-CCSD(T_0) we use cannot reliably produce benchmark level thermochemical data for transition metal containing systems. It would be surprising if the acac experiments, which were carried out by the same group, using the same apparatus and protocols, as for the metallocene experiments, were qualitatively less accurate than the latter, but some caution is warranted in the absence of confirming quantum chemical calculations.

Table 6: DFT (QZ basis) and DLPNO-CCSD(T_0) (extrapolated with TZ/QZ basis sets) adiabatic ionization energies, including thermal corrections at 350 K, as a function of metallocene and methodology. The mean absolute errors (MAE), maximum errors (MaxE), root-mean-square deviations (RMSD), and the mean signed errors (MSE) are included. All units are in kcal/mol.

	Expt.	BP86	B3LYP	B3LYP*	PBE0	TPSSh	M06	B97	B97M-V	ωB97X-V	ωB97M-V	DSD-PBEP86	DLPNO-CCSD(T_0)
$V(Cp)_2$	154.5 ± 1.5	156.92	151.44	151.22	154.11	150.76	152.35	150.74	152.03	156.88	159.03	152.29	161.29
$Cr(Cp)_2$	127.5 ± 1.5	133.21	124.17	125.70	124.08	127.02	122.60	123.95	125.06	127.74	127.00	127.68	123.81
$Mn(Cp)_2$	142.5 ± 1.5	122.75	144.62	137.85	147.51	127.66	151.31	143.03	133.93	144.64	149.40	141.62	153.53
$Fe(Cp)_2$	153.1 ± 1.5	155.24	143.21	145.25	145.67	147.35	151.83	144.28	146.96	148.78	147.72	151.24	156.19
$Co(Cp)_2$	123.5 ± 1.5	123.26	128.44	125.95	128.77	121.47	127.07	127.01	121.01	128.64	129.99	98.62	122.41
$Ni(Cp)_2$	143.8 ± 1.5	140.88	148.33	145.18	150.40	141.22	147.13	147.18	142.32	151.29	152.56	155.68	147.44
MAE		5.53	4.64	3.57	4.69	4.90	4.00	3.93	3.93	3.62	5.43	6.98	4.89
$\|MaxE\|$		19.75	9.89	7.85	7.43	14.84	8.81	8.82	8.57	7.49	8.76	24.88	11.03
RMSD		8.58	5.29	4.19	5.22	6.81	4.68	4.63	4.68	4.31	6.00	11.33	5.85
MSE		-2.11	-0.78	-2.29	0.94	-4.90	1.23	-1.45	-3.93	2.18	3.47	-2.96	3.30

Table 7: DFT (QZ basis) and DLPNO-CCSD(T_0) (extrapolated with TZ/QZ basis sets) adiabatic ionization energies as a function of acac and methodology. The mean absolute errors (MAE), maximum errors (MaxE), root-mean-square deviations (RMSD), and the mean signed errors (MSE) are included. All units are in kcal/mol.

	Expt.	BP86	B3LYP	B3LYP*	PBE0	TPSSh	M06	B97	B97M-V	ωB97X-V	ωB97M-V	DSD-PBEP86	DLPNO-CCSD(T_0)
$[V(acac)_3]^{1-}$	24.9 ± 2.4	29.11	24.30	24.28	24.21	23.11	28.42	24.67	26.37	20.66	22.60	24.60	22.50
$[Cr(acac)_3]^{1-}$	20 ± 3	7.46	10.60	8.35	10.21	2.91	15.53	11.88	1.41	8.98	10.61	14.57	7.79
$[Mn(acac)_3]^{1-}$	59 ± 5	40.15	50.31	46.30	52.09	41.48	54.84	51.75	43.78	51.87	54.55	62.67	57.13
$[Fe(acac)_3]^{1-}$	43 ± 2.4	43.11	42.86	41.74	40.85	39.75	36.30	42.11	36.62	44.25	44.50	47.04	34.05
$[Co(acac)_3]^{1-}$	47 ± 4	30.44	52.28	44.95	56.80	39.44	54.05	53.33	33.74	53.59	54.05	66.28	56.45
MAE		10.46	4.82	5.66	5.87	9.44	5.18	4.56	10.99	6.05	4.94	6.54	6.97
$\|MaxE\|$		18.85	9.40	12.70	9.80	17.52	7.05	8.12	18.59	11.02	9.39	19.28	12.21
RMSD		12.69	6.20	7.79	7.00	11.58	5.37	5.64	12.62	6.86	5.75	9.28	8.10
MSE		-8.73	-2.71	-5.66	-1.95	-9.44	-0.95	-2.03	-10.40	-2.91	-1.52	4.25	-3.20

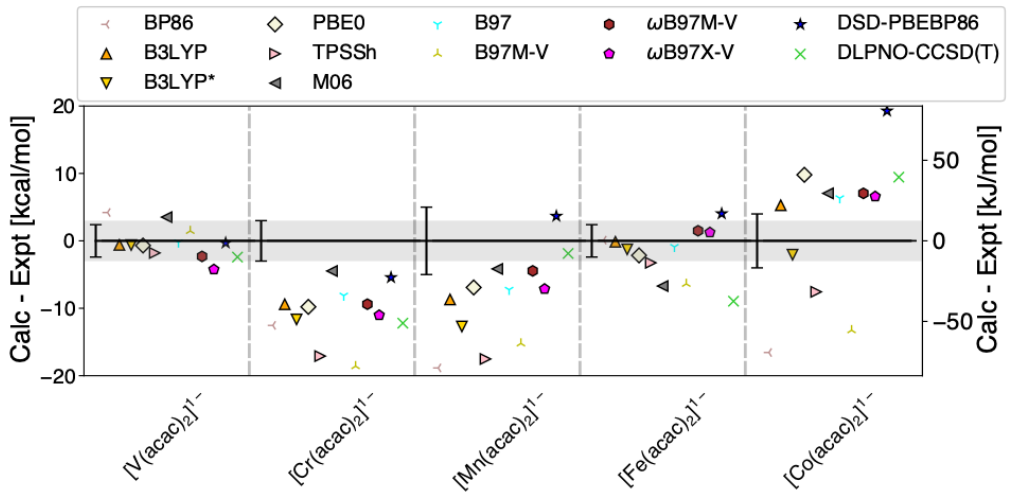

Figure 6: Performance of DFT functionals (QZ basis) and DLPNO-CCSD(T_0) (extrapolated with TZ/QZ basis sets) for prediction of experimental adiabatic gas-phase ionization energies for acac complexes. The range is limited to deviations of -20 to 20 kcal/mol. are not visible in the plot. The gray band indicates what is often given as the chemical accuracy for transition metals: 3 kcal/mol.

Reduction Potentials in Solution

Richardson and co-workers[60,61] derive THF/acetonitrile differential solvation energies for the metallocenes from their gas-phase and solution phase measurements. Therefore, we use their solvation energies to see if our results yield accurate reduction potentials. We leave the investigation of the proper simulation of solvation energies for a future publication.

The gas phase ionization energy is given by $\Delta G_{(g)}$, which is computed with ph-AFQMC and includes ideal gas free energy corrections. The differential solvation energy is given by $\Delta G_{solv,II} - \Delta G_{solv,III}$, for which we use the experimental value given in Ref. 8. Details on how the potential are derived using a thermodynamic cycle is given in the SI. Table 8 gives the resulting potentials using our best ph-AFQMC method as well as the best performing (in terms of MAE) DFT methods for the adiabatic ionization of metallocenes, namely B3LYP*. While the uncertainty of the experimentally-derived differential solvation energy clouds the interpretation of the results, ph-AFQMC clearly seems to perform well. The re-

sults show that accurate potentials can be obtained by properly describing both the gas-phase and solvation parts. Alternatively, good results can otherwise be obtained using empirical corrections[42,115–117] or error cancellation schemes.[44] Thus ph-AFQMC can be used as a microscopic approach for the computation of the gas-phase part and help isolate errors due to the solvation model.

Table 8: Computed reduction potentials (V) using the experimentally derived differential solvation energies (E_{solv}(II) - E_{solv}(III)) (kcal/mol)[59–61] as a function of metallocene and methodology for our best ph-AFQMC method as well as the best performing functional from above for the adibatic ionization energy of metallocenes B3LYP*. The mean absolute errors (MAE), maximum errors (MaxE), root-mean-square deviations (RMSD), and the mean signed errors (MSE) are included.

	Expt. Differential Solvation Energy	Expt. Potential	AFQMC/CAS CS	B3LYP*
			CAS Trial	
Units	kcal/mol	V	V	V
$V(Cp)_2$	60 ± 4	-0.31	-0.38 ± 0.19	-0.48
$Cr(Cp)_2$	36 ± 4	-0.43	-0.31 ± 0.19	-0.55
$Mn(Cp)_2$	38 ± 4	0.11	0.25 ± 0.2	-0.11
$Fe(Cp)_2$	35 ± 4	0.65	0.67 ± 0.19	0.34
$Co(Cp)_2$	38 ± 4	-0.60	-0.7 ± 0.19	-0.63
$Ni(Cp)_2$	38 ± 4	0.25	0.17 ± 0.2	0.21
MAE			0.09 ± 0.19	0.15
$\|MaxE\|$			0.14 ± 0.26	0.31
RMSD			0.09	0.18
MSE			0 ± 0.19	-0.15

V. Implications of the Results for Transition Metal Quantum Chemistry

The primary feature of the present paper is its evaluation of a significant number of quantum chemistry methods, both high level wavefunction based approaches and DFT functionals, via comparison with experimental gas phase ionization energies for two challenging series of transition metal containing molecules. All of the methods display some limitations – DFT

and DLPNO-CCSD(T_0) in accuracy, and AFQMC and more accurate versions of coupled cluster (including full CCSD(T)) in the ability to scale up to larger systems such as the acac complexes.

Nevertheless, we consider the results to be very promising in a number of dimensions. The best of the DFT methods are within striking distance of achieving "transition metal" thermochemical accuracy (2-3 kcal/mol MAEs) for the systems under study, and there is every reason to believe that progress towards this goal in the general case can be made if a larger and more relevant set of training data for transition metal containing systems is supplied to DFT developers. The effort towards enablement of AFQMC towards benchmark accuracy for large systems (i.e., $\sim$ 2000 basis functions in a TZ basis) is well underway, although nontrivial problems remain (most prominently the ability to reliably generate sufficient trial wavefunctions). Optimization of localized CCSD(T) methods such as DLPNO specifically for transition metal problems has reasonable prospects of ultimately enabling a scale up of coupled cluster based methods as well at the benchmark level of accuracy, although significant difficulties remain. See for example the recent work of Harvey and co-workers on non-heme iron complexes.[95,118] In the first work, they found that canonical CCSD(T) was in poor agreement with higher orders of coupled cluster and DMRG-CASPT2.[118] They also found that DLPNO-CCSD(T), even with tight PNO cut-offs, was not in agreement with canonical CCSD(T). In the second work, they found that these results hold for a larger system including the T_1 corrections on the DLPNO-CCSD(T) calculations.[95] Our very preliminary results for $Mn(Cp)_2$ are in fact more encouraging than these conclusions.

We see the results to date obtained by our AFQMC implementation for a series of increasingly challenging, and diverse, transition metal test cases, as illuminating a path towards both improved high level approaches and optimized DFT functionals. The excellent agreement between our AFQMC results and experiment has enabled clean benchmarking sets to be extracted from an often confusing array of experimental and theoretical papers; these can be used to test alternative single and multireference CCSD(T)-based methodology going

forward. These benchmarks should also be helpful in assessing other advanced wavefunction approaches, such as multiconfigurational pair-density functional theory (MC-PDFT),[119] other types of QMC such as diffusion Monte Carlo (DMC),[120] nonorthogonal configuration interaction with second order perturbation theory (NOCI+PT2),[121] and so on. When doing so, a balanced assessment of both accuracy and computational efficiency will be necessary.

The DFT results that we have obtained so far are consistent with our prior work. Semi-local GGA functionals appear to be incapable of obtaining reliable results for organometallic and coordination complexes of the type we have studied to date, although performance may be better for other metal-containing systems.[122] The performance of hybrid functionals of various types (including range-separated hybrids) is highly variable, with many cases yielding results that agree well with experiment, while others appear as significant outliers with errors in the 5-10 kcal/mol range. Some outliers are specific to the functional in question, but others present problems across the entire range of alternatives that we have examined, for example the Cr and Mn complexes with acac ligands. Finally, the one double hybrid functional that we tested, DSD-PBEP86, while marginally better for the acac ligands, overall displays very large average and maximum errors, in line with the poor performance in previous studies.

We conclude from these results that DFT methods for transition metals are very promising, but need to be optimized using a much larger database of benchmark experimental and "beyond CCSD(T)" theoretical results for relevant transition-metal containing systems. There are benchmark data sets such as the MOR41 and ROST61 sets of (single-reference) closed-shell and open-shell organometallic reactions[91,123] which use DLPNO-CCSD(T) as the benchmark data set, the TMC151 set of diatomic dissociation energies as well as reaction energies and barriers for typical transition metal reactions which uses a mix of experimental and CCSD(T) reference values,[124] the MOBH35 database of 35 transition metal complex reaction barrier heights computed with DLPNO-CCSD(T) in a Weizmann-1 scheme.[125] Similarly, the bond dissociation energies of various transition metal fluoride complexes have also been studied with CCSD(T) as the theoretical benchmark.[126] The spin transition properties

of several iron spin-crossover complexes have also been studied.[20] However, given the variable reliability of CCSD(T) for transition metals, especially open-shell systems, more robust benchmarks are desirable, even if more costly.

Similar large scale optimization has succeeded in reducing the number of outliers present in modern DFT functionals, such as the latest range-separated hybrids, to a very substantial degree as compared to earlier generations of functionals such as B3LYP and PBE0,[113] although it should be noted that outliers have not been entirely eliminated. We expect that similar progress can be made for transition metal containing systems. Newer approaches, such as the use of machine learning methods to create better functional forms for the DFT functional,[127–132] may also prove to be useful in the optimization process.

Going forward, we see the role of AFQMC for transition metal quantum chemistry as:

(1) Generating benchmark data sets for assessment of various coupled cluster and other wavefunction approaches, and for optimization of a next generation of DFT functionals.

(2) Obtaining results for unique, challenging systems of importance in biological and materials science, for example the Mn water splitting cluster in Photosystem II,[133,134] or the CuO planes in high T_c superconductors.[135,136]

Both of these applications will require validation of the accuracy of AFQMC methods for increasingly larger and more complex systems (e.g. those containing multiple metal centers), as well as improvements in computational efficiency to enable larger molecules, and larger data sets, to be effectively addressed. The present paper, while a step in this direction, has also been focused on pointing out the need for a true benchmark approach, via its assessment of the existing coupled cluster and DFT alternatives.

VI. Conclusions

We have developed an AFQMC protocol which yields results for the ionization of a series of metallocenes (normal oxidation state, coordinatively saturated organometallic complexes)

that are essentially within experimental error bars for both vertical and adiabatic ionization energies. The protocol has the following key ingredients: (1) A multideterminantal trial wavefunction, based on CASSCF calculations (2) The use of a CS algorithm to compute energy differences between electronic surfaces, and a PC algorithm to calculate energy differences on the same surface, namely the reorganization energy. (3) Methods for extrapolation to the CBS limit which are upgraded to a higher quality trial function as indicated by CASSCF NOONs and spin-symmetry breaking at the B3LYP level.

We are optimistic that this protocol will enable accurate AFQMC results to be obtained in the future for a wide range of challenging and important transition metal containing species, relevant to biological and materials science problems. Tests on a range of difficult systems, such as the acac series, will be necessary to confirm this hypothesis. It is important to note that failure to implement any one of these three components can degrade the AFQMC results in some cases, sometimes to a level comparable to the best DFT calculations, thus obviating the purpose of deploying a method that is much more computationally expensive.

Our investigation of DLPNO-CCSD(T_0), albeit with several technical limitations, and DFT approaches confirms our previous conclusions, that even the best of these methods, while yielding good agreement with experiment a considerable fraction of the time, are subject to frequent large uncontrolled errors for transition metal containing systems. We postulate that training DFT functionals and testing coupled cluster approaches on a greatly expanded transition metal-focused training set of benchmark data can improve this situation significantly.

Acknowledgement

B.R. acknowledges funding from the National Institute of General Medical Sciences of the National Institutes of Health under award number F32GM136105. D.R.R. acknowledges funding from NSF CHE-1954791. S.Z. acknowledges funding from DOE DE-SC0001303.

J.S. acknowledges funding from the National Institute of General Medical Sciences of the National Institutes of Health under award number F32GM142231. An award of computer time was provided by the Innovative and Novel Computational Impact on Theory and Experiment (INCITE) program. This research used resources of the Oak Ridge Leadership Computing Facility at the Oak Ridge National Laboratory, which is supported by the Office of Science of the U.S. Department of Energy under Contract No. DE-AC05-00OR22725. This work used the Extreme Science and Engineering Discovery Environment (XSEDE), which is supported by National Science Foundation grant number ACI-1548562. In particular, we used San Diego Computing Center's Comet and Expanse resources under grant number TG-CHE190007 and allocation ID COL151. The Flatiron Institute is a division of the Simons Foundation. We would like to thank Joonho Lee, the QMC group at the Flatiron Institute, Prof. Martin Head-Gordon, Diptarka Hait, and Elvira Sayfutyarova for helpful discussions.

Supporting Information Available

Tabulated DLPNO-CCSD(T_0), ph-AFQMC vertical and adiabatic energies in the TZ basis set, basis set extrapolation corrections for all methods, scaling factors for the CBS extrapolations, free energy corrections, active space information, CASSCF energies, NOON's, $\langle S^2 \rangle$ values, metal spin density values, details on the convergence of ph-AFQMC with respect to active space, details on the DFT integration grids, stability calculations, how CBS extrapolations are done for DLPNO-CCSD(T_0), a workflow in terms of how other calculations complement the ph-AFQMC calculations, alternate experimental values, additional methodology details for ph-AFQMC, details on how potentials are calculated in solution, details on the calculation of statistical measures to compare to experiment, explanation of CS algorithms, ionization energies including diffuse functions on certain atoms, results with D4 dispersion, B3LYP M-Cp distances in the metallocenes, literature experimental homolytic

bond dissociation energies for the metallocenes, tests of DLPNO-CCSD(T) PNO cut-off and (T) treatment, reorganization energies with one center approximation off and additional references (PDF) as well as B3LYP-optimized coordinates for transition metal complexes (TXT).

References

(1) Friesner, R. A. Ab Initio Quantum Chemistry: Methodology and Applications. *Proc. Nat. Acad. Sci.* **2005**, *102*, 6648–6653.

(2) Curtiss, L. A.; Raghavachari, K.; Redfern, P. C.; Pople, J. A. Assessment of Gaussian-3 and Density Functional Theories for a Larger Experimental Test Set. *J. Chem. Phys.* **2000**, *112*, 7374–7383.

(3) Curtiss, L. A.; Raghavachari, K.; Redfern, P. C.; Baboul, A. G.; Pople, J. A. Gaussian-3 Theory Using Coupled Cluster Energies. *Chem. Phys. Lett.* **1999**, *314*, 101–107.

(4) Perdew, J. P.; Burke, K.; Ernzerhof, M. Generalized Gradient Approximation Made Simple. *Phys. Rev. Lett.* **1996**, *77*, 3865.

(5) Becke, A. D. Density-Functional Thermochemistry. III. The Role of Exact Exchange. *J. Chem. Phys.* **1993**, *98*, 5648–5652.

(6) Vosko, S. H.; Wilk, L.; Nusair, M. Accurate Spin-Dependent Electron Liquid Correlation Energies for Local Spin Density Calculations: A Critical Analysis. *Can. J. Phys.* **1980**, *58*, 1200–1211.

(7) Lee, C.; Yang, W.; Parr, R. G. Development of the Colle-Salvetti Correlation-Energy Formula Into a Functional of the Electron Density. *Phys. Rev. B* **1988**, *37*, 785.

(8) Becke, A. D. Density-Functional Thermochemistry. V. Systematic Optimization of Exchange-Correlation Functionals. *J. Chem. Phys.* **1997**, *107*, 8554–8560.

(9) Schmider, H. L.; Becke, A. D. Optimized Density Functionals From the Extended G2 Test Set. *J. Chem. Phys.* **1998**, *108*, 9624–9631.

(10) Adamo, C.; Barone, V. Toward Reliable Density Functional Methods Without Adjustable Parameters: The PBE0 Model. *J. Chem. Phys.* **1999**, *110*, 6158–6170.

(11) Ernzerhof, M.; Perdew, J. P. Generalized Gradient Approximation to the Angle-and System-Averaged Exchange Hole. *J. Chem. Phys.* **1998**, *109*, 3313–3320.

(12) Hamprecht, F. A.; Cohen, A. J.; Tozer, D. J.; Handy, N. C. Development and Assessment of New Exchange-Correlation Functionals. *J. Chem. Phys.* **1998**, *109*, 6264–6271.

(13) Ma, Q.; Schwilk, M.; Koppl, C.; Werner, H.-J. Scalable Electron Correlation Methods. 4. Parallel Explicitly Correlated Local Coupled Cluster With Pair Natural Orbitals (PNO-LCCSD-F12). *J. Chem. Comput. Chem.* **2017**, *13*, 4871–4896.

(14) Ma, Q.; Werner, H.-J. Accurate Intermolecular Interaction Energies Using Explicitly Correlated Local Coupled Cluster Methods [PNO-LCCSD (T)-F12]. *J. Chem. Theory Comput.* **2019**, *15*, 1044–1052.

(15) Liakos, D. G.; Sparta, M.; Kesharwani, M. K.; Martin, J. M. L.; Neese, F. Exploring the Accuracy Limits of Local Pair Natural Orbital Coupled-Cluster Theory. *J. Chem. Theory Comput.* **2015**, *11*, 1525–1539.

(16) Riplinger, C.; Sandhoefer, B.; Hansen, A.; Neese, F. Natural Triple Excitations in Local coupled Cluster Calculations with Pair Natural Orbitals. *J. Chem. Phys.* **2013**, *139*, 134101.

(17) Riplinger, C.; Pinski, P.; Becker, U.; Valeev, E. F.; Neese, F. Sparse Maps – A Systematic Infrastructure for Reduced-Scaling Electronic Structure Methods. II. Linear Scaling Domain Based Pair Natural Orbital Coupled Cluster Theory. *J. Chem. Phys.* **2016**, *144*, 024109.

(18) Guo, Y.; Riplinger, C.; Becker, U.; Liakos, D. G.; Minenkov, Y.; Cavallo, L.; Neese, F. Communication: An Improved Linear Scaling Perturbative Triples Correction for the Domain Based Local Pair-Natural Orbital Based Singles and Doubles Coupled Cluster Method [DLPNO-CCSD(T)]. *J. Chem. Phys.* **2018**, *148*, 011101.

(19) Saitow, M.; Becker, U.; Riplinger, C.; Valeev, E. F.; Neese, F. A New Near-Linear Scaling, Efficient and Accurate, Open-Shell Domain-Based Local Pair Natural Orbital Coupled Cluster Singles and Doubles Theory. *J. Chem. Phys.* **2017**, *146*, 164105.

(20) Flöser, B. M.; Guo, Y.; Riplinger, C.; Tuczek, F.; Neese, F. Detailed Pair Natural Orbital–based Coupled Cluster Studies of Spin Crossover Energetics. *J. Chem. Theory Comput.* **2020**, *16*, 2224–2235.

(21) Lin, H.; Truhlar, D. G. QM/MM: What Have We Learned, Where Are We, and Where Do We Go From Here? *Theor. Chem. Acc.* **2007**, *117*, 185.

(22) Bistoni, G.; Polyak, I.; Sparta, M.; Thiel, W.; Neese, F. Toward Accurate QM/MM Reaction Barriers With Large QM Regions Using Domain Based Pair Natural Orbital Coupled Cluster Theory. *J. Chem. Theory Comput.* **2018**, *14*, 3524–3531.

(23) Shee, J.; Arthur, E. J.; Zhang, S.; Reichman, D. R.; Friesner, R. A. Phaseless Auxiliary-Field Quantum Monte Carlo on Graphical Processing Units. *J. Chem. Theory Comput.* **2018**, *14*, 4109–4121.

(24) Jiang, W.; DeYonker, N. J.; Determan, J. J.; Wilson, A. K. Toward Accurate Theoretical Thermochemistry of First Row Transition Metal Complexes. *J. Phys. Chem. A* **2011**, *116*, 870–885.

(25) Xu, X.; Zhang, W.; Tang, M.; Truhlar, D. G. Do Practical Standard Coupled Cluster Calculations Agree Better than Kohn–Sham Calculations with Currently Available Functionals When Compared to the Best Available Experimental Data for Dissociation

Energies of Bonds to 3d Transition Metals? *J. Chem. Theory Comput.* **2015**, *11*, 2036–2052.

(26) Cheng, L.; Gauss, J.; Ruscic, B.; Armentrout, P. B.; Stanton, J. F. Bond Dissociation Energies for Diatomic Molecules Containing 3d Transition Metals: Benchmark Scalar-Relativistic Coupled-Cluster Calculations for 20 Molecules. *J. Chem. Theory Comput.* **2017**, *13*, 1044–1056.

(27) Fang, Z.; Vasiliu, M.; Peterson, K. A.; Dixon, D. A. Prediction of Bond Dissociation Energies/Heats of Formation for Diatomic Transition Metal Compounds: CCSD(T) Works. *J. Chem. Theory Comput.* **2017**, *13*, 1057–1066.

(28) Aoto, Y. A.; de Lima Batista, A. P.; Köhn, A.; de Oliveira-Filho, A. G. S. How to Arrive at Accurate Benchmark Values for Transition Metal Compounds: Computation or Experiment? *J. Chem. Theory Comput.* **2017**, *13*, 5291–5316.

(29) Shee, J.; Rudshteyn, B.; Arthur, E. J.; Zhang, S.; Reichman, D. R.; Friesner, R. A. On Achieving High Accuracy in Quantum Chemical Calculations of 3d Transition Metal-Containing Systems: A Comparison of Auxiliary-Field Quantum Monte Carlo with Coupled Cluster, Density Functional Theory, and Experiment for Diatomic Molecules. *J. Chem. Theory Comput.* **2019**, *15*, 2346–2358.

(30) Williams, K. T. et al. Direct Comparison of Many-Body Methods for Realistic Electronic Hamiltonians. *Phys. Rev. X* **2020**, *10*, 011041.

(31) Bross, D. H.; Hill, J. G.; Werner, H.-J.; Peterson, K. A. Explicitly Correlated Composite Thermochemistry of Transition Metal Species. *J. Chem. Phys.* **2013**, *139*, 094302.

(32) Manivasagam, S.; Laury, M. L.; Wilson, A. K. Pseudopotential-Based Correlation Consistent Composite Approach (Rp-ccCA) for First-and Second-Row Transition Metal Thermochemistry. *J. Phys. Chem. A* **2015**, *119*, 6867–6874.

(33) Jiang, W.; Laury, M. L.; Powell, M.; Wilson, A. K. Comparative Study of Single and Double Hybrid Density Functionals for the Prediction of 3d Transition Metal Thermochemistry. *J. Comput. Theory Comput.* **2012**, *8*, 4102–4111.

(34) Zhang, W.; Truhlar, D. G.; Tang, M. Tests of Exchange-Correlation Functional Approximations Against Reliable Experimental Data for Average Bond Energies of 3d Transition Metal Compounds. *J. Chem. Theory Comput.* **2013**, *9*, 3965–3977.

(35) Moltved, K. A.; Kepp, K. P. Chemical Bond Energies of 3d Transition Metals Studied by Density Functional Theory. *J. Chem. Theory Comput.* **2018**,

(36) Carlson, R. K.; Li Manni, G.; Sonnenberger, A. L.; Truhlar, D. G.; Gagliardi, L. Multiconfiguration Pair-Density Functional Theory: Barrier Heights and Main Group and Transition Metal Energetics. *J. Chem. Theor. Comp.* **2014**, *11*, 82–90.

(37) Bao, J. L.; Odoh, S. O.; Gagliardi, L.; Truhlar, D. G. Predicting Bond Dissociation Energies of Transition-Metal Compounds by Multiconfiguration Pair-Density Functional Theory and Second-Order Perturbation Theory Based on Correlated Participating Orbitals and Separated Pairs. *J. Chem. Theory Comput.* **2017**, *13*, 616–626.

(38) Bao, J. L.; Zhang, X.; Xu, X.; Truhlar, D. G. Predicting Bond Dissociation Energy and Bond Length for Bimetallic Diatomic Molecules: A Challenge for Electronic Structure Theory. *Phys. Chem. Chem. Phys.* **2017**, *19*, 5839–5854.

(39) Sharkas, K.; Gagliardi, L.; Truhlar, D. G. Multiconfiguration Pair-Density Functional Theory and Complete Active Space Second Order Perturbation Theory. Bond Dissociation Energies of FeC, NiC, FeS, NiS, FeSe, and NiSe. *J. Phys. Chem. A* **2017**, *121*, 9392–9400.

(40) Tran, L. N.; Iskakov, S.; Zgid, D. Spin-Unrestricted Self-Energy Embedding Theory. *J. Phys. Chem. Lett.* **2018**,

(41) Hughes, T. F.; Friesner, R. A. Development of Accurate DFT Methods for Computing Redox Potentials of Transition Metal Complexes: Results for Model Complexes and Application to Cytochrome P450. *J. Chem. Theory Comput.* **2012**, *8*, 442–459.

(42) Coskun, D.; Jerome, S. V.; Friesner, R. A. Evaluation of the Performance of the B3LYP, PBE0, and M06 DFT Functionals, and DBLOC-Corrected Versions, in the Calculation of Redox Potentials and Spin Splittings for Transition Metal Containing Systems. *J. Chem. Theory Comput.* **2016**, *12*, 1121–1128.

(43) Roy, L. E.; Jakubikova, E.; Guthrie, M. G.; Batista, E. R. Calculation of One-Electron Redox Potentials Revisited. Is It Possible to Calculate Accurate Potentials With Density Functional Methods? *J. Phys. Chem. A* **2009**, *113*, 6745–6750.

(44) Konezny, S. J.; Doherty, M. D.; Luca, O. R.; Crabtree, R. H.; Soloveichik, G. L.; Batista, V. S. Reduction of Systematic Uncertainty in DFT Redox Potentials of Transition-Metal Complexes. *J. Phys. Chem. C* **2012**, *116*, 6349–6356.

(45) Green, J. C. *Bonding Problems*; Springer, 1981; pp 37–112.

(46) Zhang, S.; Krakauer, H. Quantum Monte Carlo Method Using Phase-Free Random Walks With Slater Determinants. *Phys. Rev. Lett.* **2003**, *90*, 136401.

(47) Al-Saidi, W. A.; Zhang, S.; Krakauer, H. Auxiliary-Field Quantum Monte Carlo Calculations of Molecular Systems With a Gaussian Basis. *J. Chem. Phys.* **2006**, *124*, 224101.

(48) Motta, M.; Zhang, S. Ab initio Computations of Molecular Systems by the Auxiliary-Field Quantum Monte Carlo Method. *WIRES Comput. Mol. Sci.* **2018**, *8*, e1364.

(49) Bartlett, R. J.; Musiał, M. Coupled-Cluster Theory in Quantum Chemistry. *Rev. Mod. Phys.* **2007**, *79*, 291.

(50) Shi, H.; Zhang, S. Some Recent Developments in Auxiliary-Field Quantum Monte Carlo for Real Materials. *J. Chem. Phys.* **2021**, *154*, 024107.

(51) Shee, J.; Zhang, S.; Reichman, D. R.; Friesner, R. A. Chemical Transformations Approaching Chemical Accuracy via Correlated Sampling in Auxiliary-Field Quantum Monte Carlo. *J. Chem. Theory Comput.* **2017**, *13*, 2667–2680.

(52) Malone, F. D.; Zhang, S.; Morales, M. A. Accelerating Auxiliary-Field Quantum Monte Carlo Simulations of Solids with Graphical Processing Units. *J. Chem. Theory Comput.* **2020**, *16*, 4286–4297.

(53) Lee, J.; Malone, F. D.; Morales, M. A. Utilizing Essential Symmetry Breaking in Auxiliary-Field Quantum Monte Carlo: Application to the Spin Gaps of the C_{36} Fullerene and an Iron Porphyrin Model Complex. *J. Chem. Theory Comput.* **2020**, *16*, 3019–3027.

(54) Rudshteyn, B.; Coskun, D.; Weber, J. L.; Arthur, E. J.; Zhang, S.; Reichman, D. R.; Friesner, R. A.; Shee, J. Predicting Ligand-Dissociation Energies of 3d Coordination Complexes with Auxiliary-Field Quantum Monte Carlo. *J. Chem. Theory Comput.* **2020**, *16*, 3041–3054.

(55) Weber, J. L.; Churchill, E. M.; Jockusch, S.; Arthur, E. J.; Pun, A. B.; Zhang, S.; Friesner, R. A.; Campos, L. M.; Reichman, D. R.; Shee, J. In Silico Prediction of Annihilators for Triplet–Triplet Annihilation Upconversion via Auxiliary-Field Quantum Monte Carlo. *Chem. Sci.* **2021**, *12*, 1068–1079.

(56) Morse, M. D. Predissociation Measurements of Bond Dissociation Energies. *Acc. Chem. Res.* **2019**, *52*, 119–126.

(57) Hait, D.; Tubman, N. M.; Levine, D. S.; Whaley, K. B.; Head-Gordon, M. What Levels of Coupled Cluster Theory Are Appropriate for Transition Metal Systems? A

Study Using Near Exact Quantum Chemical Values for 3d Transition Metal Binary Compounds. *J. Chem Theory Comput.* **2019**, *15*, 5370–5385.

(58) Pavlishchuk, V. V.; Addison, A. W. Conversion Constants for Redox Potentials Measured Versus Different Reference Electrodes in Acetonitrile Solutions at 25 °C. *Inorganica Chimica Acta* **2000**, *298*, 97–102.

(59) Richardson, D. E. *Organometallic Ion Chemistry*; Springer, 1996; pp 259–282.

(60) Ryan, M. F.; Eyler, J. R.; Richardson, D. E. Adiabatic Ionization Energies, Bond Disruption Enthalpies, and Solvation Free Energies for Gas-Phase Metallocenes and Metallocenium Ions. *J. Am. Chem. Soc.* **1992**, *114*, 8611–8619.

(61) Ryan, M. F.; Richardson, D. E.; Lichtenberger, D. L.; Gruhn, N. E. Gas-Phase Ionization Energetics, Electron-Transfer Kinetics, and Ion Solvation Thermochemistry of Decamethylmetallocenes, Chromocene, and Cobaltocene. *Organometallics* **1994**, *13*, 1190–1199.

(62) Cauletti, C.; Green, J. C.; Kelly, M. R.; Powell, P.; van Tilborg, J.; Robbins, J.; Smart, J. Photoelectron Spectra of Metallocenes. *J. Elec. Spec. Rel. Phen.* **1980**, *19*, 327–353.

(63) Crabtree, R. H. *The Organometallic Chemistry of the Transition Metals*; John Wiley & Sons, 2009.

(64) Ishimura, K.; Hada, M.; Nakatsuji, H. Ionized and Excited States of Ferrocene: Symmetry Adapted Cluster–Configuration–Interaction Study. *J. Chem. Phys.* **2002**, *117*, 6533–6537.

(65) Huntington, L. M. J.; Nooijen, M. Application of Multireference Equation of Motion Coupled-Cluster Theory to Transition Metal Complexes and an Orbital Selection

Scheme for the Efficient Calculation of Excitation Energies. *J. Chem. Phys.* **2015**, *142*, 194111.

(66) Huntington, L. M. J.; Demel, O.; Nooijen, M. Benchmark Applications of Variations of Multireference Equation of Motion Coupled-Cluster Theory. *J. Chem. Theory Comput.* **2016**, *12*, 114–132.

(67) Phung, Q. M.; Vancoillie, S.; Pierloot, K. A Multiconfigurational Perturbation Theory and Density Functional Theory Study on the Heterolytic Dissociation Enthalpy of First-Row Metallocenes. *J. Chem. Theory Comput.* **2012**, *8*, 883–892.

(68) Namazian, M.; Lin, C. Y.; Coote, M. L. Benchmark Calculations of Absolute Reduction Potential of Ferricinium/Ferrocene Couple in Nonaqueous Solutions. *J. Chem. Theory Comput.* **2010**, *6*, 2721–2725.

(69) Shee, J.; Loipersberger, M.; Hait, D.; Lee, J.; Head-Gordon, M. Revealing the Nature of Electron Correlation in Transition Metal Complexes With Symmetry-Breaking and Chemical Intuition. *J. Chem. Phys.* **2021**, *154*, 194109.

(70) Sharpe, P.; Eyler, J. R.; Richardson, D. E. Free Energies of Electron Attachment to Tris (Acetylacetonate) and Tris (Hexafluoroacetylacetonate) Transition-Metal Complexes in the Gas Phase: Experimental Results and Ligand Field Analysis. *Inorg. Chem.* **1990**, *29*, 2779–2787.

(71) Sharpe, P.; Richardson, D. E. Metal-Ligand Bond Energies and Solvation Energies for Gas-Phase Transition-Metal Tris (Acetylacetonate) Complexes and Their Negative Ions. *J. Am. Chem. Soc.* **1991**, *113*, 8339–8346.

(72) Shee, J.; Arthur, E. J.; Zhang, S.; Reichman, D. R.; Friesner, R. A. Singlet–Triplet Energy Gaps of Organic Biradicals and Polyacenes with Auxiliary-Field Quantum Monte Carlo. *J. Chem. Theory Comput.* **2019**, *15*, 4924–4932.

(73) Nawa, K.; Kitaoka, Y.; Nakamura, K.; Imamura, H.; Akiyama, T.; Ito, T.; Weinert, M. Search for the Ground-State Electronic Configurations of Correlated Organometallic Metallocenes From Constraint Density Functional Theory. *Phys. Rev. B* **2016**, *94*, 035136.

(74) Evans, S.; Green, M. L. H.; Jewitt, B.; Orchard, A. F.; Pygall, C. F. Electronic Structure of Metal Complexes Containing π-Cyclopentadienyl and Related Ligands. Part 1.—He (I) Photoelectron Spectra of Some Closed-Shell Metallocenes. *J. Chem. Soc., Faraday Trans. 2* **1972**, *68*, 1847–1865.

(75) Evans, S.; Green, M. L. H.; Jewitt, B.; King, G. H.; Orchard, A. F. Electronic Structures of Metal Complexes Containing the Π-Cyclopentadienyl and Related Ligands. Part 2.—He I Photoelectron Spectra of the Open-Shell Metallocenes. *J. Chem. Soc., Faraday Trans. 2* **1974**, *70*, 356–376.

(76) Gordon, K. R.; Warren, K. D. Spectroscopic and Magnetic Studies of the 3d Metallocenes. *Inorg. Chem.* **1978**, *17*, 987–994.

(77) Rettig, M. F.; Drago, R. S. Electron Delocalization in Paramagnetic Metallocenes. I. Nuclear Magnetic Resonance Contact Shifts. *J. Am. Chem. Soc.* **1969**, *91*, 1361–1370.

(78) Xu, Z.-F.; Xie, Y.; Feng, W.-L.; Schaefer, H. F. Systematic Investigation of Electronic and Molecular Structures for the First Transition Metal Series Metallocenes M $(C_5H_5)_2$ (M= V, Cr, Mn, Fe, Co, and Ni). *J. Phys. Chem. A* **2003**, *107*, 2716–2729.

(79) Trasatti, S., et al. The Absolute Electrode Potential: An Explanatory Note (Recommendations 1986). *Pure Appl. Chem* **1986**, *58*, 955–966.

(80) Cramer, C. J. *Essentials of Computational Chemistry: Theories and Models*; John Wiley & Sons, 2013.

(81) Dunning, T. H. Gaussian Basis Sets for Use in Correlated Molecular Calculations. I. The Atoms Boron Through Neon and Hydrogen. *J. Chem. Phys.* **1989**, *90*.

(82) Woon, D. E.; Dunning, T. H. Gaussian Basis Sets for Use in Correlated Molecular Calculations. III. The Atoms Aluminum Through Argon. *J. Chem. Phys.* **1993**, *98*.

(83) de Jong, W. A.; Harrison, R. J.; Dixon, D. A. Parallel Douglas-Kroll Energy and Gradients in NWChem: Estimating Scalar Relativistic Effects Using Douglas-Kroll Contracted Basis Sets. *J. Chem. Phys.* **2001**, *114*.

(84) Balabanov, N. B.; Peterson, K. A. Systematically Convergent Basis Sets for Transition Metals. I. All-Electron Correlation Consistent Basis Sets for the 3d Elements Sc–Zn. *J. Chem. Phys.* **2005**, *123*, 064107.

(85) Pantazis, D. A.; Chen, X.-Y.; Landis, C. R.; Neese, F. All-Electron Scalar Relativistic Basis Sets for Third-Row Transition Metal Atoms. *J. Chem. Theory Comput.* **2008**, *4*, 908–919.

(86) Neese, F. The ORCA Program System. *WIRES Comput. Mol. Sci.* **2012**, *2*, 73–78.

(87) Caldeweyher, E.; Bannwarth, C.; Grimme, S. Extension of the D3 Dispersion Coefficient Model. *J. Chem. Phys.* **2017**, *147*, 034112.

(88) Purwanto, W.; Krakauer, H.; Virgus, Y.; Zhang, S. Assessing Weak Hydrogen Binding on Ca^+ Centers: An Accurate Many-Body Study With Large Basis Sets. *J. Chem. Phys.* **2011**, *135*, 164105.

(89) Altun, A.; Saitow, M.; Neese, F.; Bistoni, G. Local Energy Decomposition of Open-Shell Molecular Systems in the Domain-Based Local Pair Natural Orbital Coupled Cluster Framework. *J. Chem. Theory Comput.* **2019**, *15*, 1616–1632.

(90) Minenkov, Y.; Bistoni, G.; Riplinger, C.; Auer, A. A.; Neese, F.; Cavallo, L. Pair Natural Orbital and Canonical Coupled Cluster Reaction Enthalpies Involving Light to

Heavy Alkali and Alkaline Earth Metals: The Importance of Sub-Valence Correlation. *Phys. Chem. Chem. Phys.* **2017**, *19*, 9374–9391.

(91) Dohm, S.; Hansen, A.; Steinmetz, M.; Grimme, S.; Checinski, M. P. Comprehensive Thermochemical Benchmark Set of Realistic Closed-Shell Metal Organic Reactions. *J. Chem. Theory Comput.* **2018**, *14*, 2596–2608.

(92) Efremenko, I.; Martin, J. M. L. Coupled Cluster Benchmark of New Density Functionals and of Domain Pair Natural Orbital Methods: Mechanisms of Hydroarylation and Oxidative Coupling Catalyzed by Ru(II) Chloride Carbonyls. AIP Conf. Proc. 2019; p 030005.

(93) Altun, A.; Neese, F.; Bistoni, G. Extrapolation to the Limit of a Complete Pair Natural Orbital Space in Local Coupled-Cluster Calculations. *J. Chem. Theory Comput.* **2020**, *16*, 6142–6149.

(94) Helgaker, T.; Klopper, W.; Koch, H.; Noga, J. Basis-Set Convergence of Correlated Calculations on Water. *J. Chem. Phys.* **1997**, *106*, 9639–9646.

(95) Feldt, M.; Martín-Fernández, C.; Harvey, J. N. Energetics of Non-Heme Iron Reactivity: Can Ab Initio Calculations Provide the Right Answer? *Phys. Chem. Chem. Phys.* **2020**, *22*, 23908–23919.

(96) Sun, Q.; Berkelbach, T. C.; Blunt, N. S.; Booth, G. H.; Guo, S.; Li, Z.; Liu, J.; McClain, J. D.; Sayfutyarova, E. R.; Sharma, S.; Wouters, S.; Chan, G. K. PySCF: the Python–Based Simulations of Chemistry Framework. *WIRES Comput. Mol. Sci. 8*, e1340.

(97) Liu, W.; Peng, D. Exact Two-Component Hamiltonians Revisited. *J. Chem. Phys.* **2009**, *131*, 031104.

(98) Ma, F.; Zhang, S.; Krakauer, H. Excited State Calculations in Solids by Auxiliary-Field Quantum Monte Carlo. *New J. Phys.* **2013**, *15*, 093017.

(99) Purwanto, W.; Al-Saidi, W.; Krakauer, H.; Zhang, S. Eliminating Spin Contamination in Auxiliary-Field Quantum Monte Carlo: Realistic Potential Energy Curve of F_2. *J. Chem. Phys.* **2008**, *128*, 114309.

(100) Roos, B. O.; Lindh, R.; Malmqvist, P.-Å.; Veryazov, V.; Widmark, P.-O. New Relativistic ANO Basis Sets for Transition Metal Atoms. *J. Phys. Chem. A* **2005**, *109*, 6575–6579.

(101) Sayfutyarova, E. R.; Sun, Q.; Chan, G. K.-L.; Knizia, G. Automated Construction of Molecular Active Spaces From Atomic Valence Orbitals. *J. Chem. Theory Comput.* **2017**, *13*, 4063–4078.

(102) Becke, A. D. Density-functional Exchange-Energy Approximation with Correct Asymptotic Behavior. *Phys. Rev. A* **1988**, *38*, 3098.

(103) Perdew, J. P. Density-Functional Approximation for the Correlation Energy of the Inhomogeneous Electron Gas. *Phys. Rev. B* **1986**, *33*, 8822.

(104) Salomon, O.; Reiher, M.; Hess, B. A. Assertion and Validation of the Performance of the B3LYP* Functional for the First Transition Metal Row and the G2 Test Set. *J. Chem. Phys.* **2002**, *117*, 4729–4737.

(105) Zhao, Y.; Truhlar, D. G. The M06 Suite of Density Functionals for Main Group Thermochemistry, Thermochemical Kinetics, Noncovalent Interactions, Excited States, and Transition Elements: Two New Functionals and Systematic Testing of Four M06-Class Functionals and 12 Other Functionals. *Theor. Chem. Acc.* **2008**, *120*, 215–241.

(106) Tao, J.; Perdew, J. P.; Staroverov, V. N.; Scuseria, G. E. Climbing the Density Func-

tional Ladder: Nonempirical Meta–Generalized Gradient Approximation Designed for Molecules and Solids. *Phys. Rev. Lett.* **2003**, *91*, 146401.

(107) Staroverov, V. N.; Scuseria, G. E.; Tao, J.; Perdew, J. P. Comparative Assessment of a New Nonempirical Density Functional: Molecules and Hydrogen-Bonded Complexes. *J. Chem. Phys.* **2003**, *119*, 12129–12137.

(108) Mardirossian, N.; Head-Gordon, M. Mapping the Genome of Meta-Generalized Gradient Approximation Density Functionals: The Search for B97M-V. *J. Chem. Phys* **2015**, *142*, 074111.

(109) Mardirossian, N.; Head-Gordon, M. ωB97M-V: A Combinatorially Optimized, Range-Separated Hybrid, Meta-GGA Density Functional With VV10 Nonlocal Correlation. *J. Chem. Phys.* **2016**, *144*, 214110.

(110) Mardirossian, N.; Head-Gordon, M. ωB97X-V: A 10-Parameter, Range-Separated Hybrid, Generalized Gradient Approximation Density Functional With Nonlocal Correlation, Designed by a Survival-of-the-Fittest Strategy. *Phys. Chem. Chem. Phys.* **2014**, *16*, 9904–9924.

(111) Kozuch, S.; Martin, J. M. DSD-PBEP86: In Search of the Best Double-Hybrid DFT With Spin-Component Scaled MP2 and Dispersion Corrections. *Phys. Chem. Chem. Phys.* **2011**, *13*, 20104–20107.

(112) Kozuch, S.; Martin, J. M. Spin-Component-Scaled Double Hybrids: An Extensive Search for the Best Fifth-Rung Functionals Blending DFT and Perturbation Theory. *J. Comput. Chem.* **2013**, *34*, 2327–2344.

(113) Mardirossian, N.; Head-Gordon, M. Thirty Years of Density Functional Theory in Computational Chemistry: An Overview and Extensive Assessment of 200 Density Functionals. *Mol. Phys.* **2017**, *115*, 2315–2372.

(114) Hughes, T. F.; Friesner, R. A. Correcting Systematic Errors in DFT Spin-Splitting Energetics for Transition Metal Complexes. *J. Chem. Theory Comput.* **2011**, *7*, 19–32.

(115) Friesner, R. A.; Knoll, E. H.; Cao, Y. A Localized Orbital Analysis of the Thermochemical Errors in Hybrid Density Functional Theory: Achieving Chemical Accuracy via a Simple Empirical Correction Scheme. *J. Chem. Phys.* **2006**, *125*, 124107.

(116) Friesner, R. A.; Jerome, S. V. Localized Orbital Corrections for Density Functional Calculations on Transition Metal Containing Systems. *Coord. Chem. Rev.* **2017**, *344*, 205–213.

(117) Jerome, S. V.; Hughes, T. F.; Friesner, R. A. Successful Application of the DBLOC Method to the Hydroxylation of Camphor by Cytochrome p450. *Protein Sci.* **2016**, *25*, 277–285.

(118) Feldt, M.; Phung, Q. M.; Pierloot, K.; Mata, R. A.; Harvey, J. N. Limits of Coupled-Cluster Calculations for Non-Heme Iron Complexes. *J. Chem. Theory Comput.* **2019**, *15*, 922–937.

(119) Gagliardi, L.; Truhlar, D. G.; Li Manni, G.; Carlson, R. K.; Hoyer, C. E.; Bao, J. L. Multiconfiguration Pair-Density Functional Theory: A New Way to Treat Strongly Correlated Systems. *Acc. Chem. Res.* **2016**, *50*, 66–73.

(120) Doblhoff-Dier, K.; Meyer, J.; Hoggan, P. E.; Kroes, G.-J.; Wagner, L. K. Diffusion Monte Carlo for Accurate Dissociation Energies of 3d Transition Metal Containing Molecules. *J. Chem. Theory Comput.* **2016**, *12*, 2583–2597.

(121) Burton, H. G. A.; Thom, A. J. W. Reaching Full Correlation through Nonorthogonal Configuration Interaction: A Second-Order Perturbative Approach. *J. Chem. Theory Comput.* **2020**, *16*, 5586–5600.

(122) Cramer, C. J.; Włoch, M.; Piecuch, P.; Puzzarini, C.; Gagliardi, L. Theoretical Models on the Cu_2O_2 Torture Track: Mechanistic Implications for Oxytyrosinase and Small-Molecule Analogues. *J. Phys. Chem. A.* **2006**, *110*, 1991–2004.

(123) Maurer, L. R.; Bursch, M.; Grimme, S.; Hansen, A. Assessing Density Functional Theory for Chemically Relevant Open-Shell Transition Metal Reactions. *J. Chem. Theory Comput.* **2021**,

(124) Chan, B.; Gill, P. M. W.; Kimura, M. Assessment of DFT Methods for Transition Metals with the TMC151 Compilation of Data Sets and Comparison with Accuracies for Main-Group Chemistry. *J. Chem. Theor. Comp* **2019**,

(125) Iron, M. A.; Janes, T. Evaluating Transition Metal Barrier Heights With the Latest Density Functional Theory Exchange–Correlation Functionals: The MOBH35 Benchmark Database. *J. Phys. Chem. A* **2019**, *123*, 3761–3781.

(126) Bistoni, G.; Riplinger, C.; Minenkov, Y.; Cavallo, L.; Auer, A. A.; Neese, F. Treating Subvalence Correlation Effects in Domain Based Pair Natural Orbital Coupled Cluster Calculations: An out-of-the-Box Approach. *J. Chem. Theory Comput.* **2017**, *13*, 3220–3227.

(127) Snyder, J. C.; Rupp, M.; Hansen, K.; Müller, K.-R.; Burke, K. Finding Density Functionals With Machine Learning. *Phys. Rev. Lett.* **2012**, *108*, 253002.

(128) Schmidt, J.; Benavides-Riveros, C. L.; Marques, M. A. Machine Learning the Physical Nonlocal Exchange–Correlation Functional of Density-Functional Theory. *J. Phys. Chem. Lett.* **2019**, *10*, 6425–6431.

(129) Nagai, R.; Akashi, R.; Sugino, O. Completing Density Functional Theory by Machine Learning Hidden Messages From Molecules. *Npj Comput. Mater.* **2020**, *6*, 1–8.

(130) Dick, S.; Fernandez-Serra, M. Machine Learning Accurate Exchange and Correlation Functionals of the Electronic Density. *Nat. Commun.* **2020**, *11*, 1–10.

(131) Meyer, R.; Weichselbaum, M.; Hauser, A. W. Machine Learning Approaches Toward Orbital-Free Density Functional Theory: Simultaneous Training on the Kinetic Energy Density Functional and Its Functional Derivative. *J. Chem. Theory Comput.* **2020**, *16*, 5685–5694.

(132) Kalita, B.; Li, L.; McCarty, R. J.; Burke, K. Learning to Approximate Density Functionals. *Acc. Chem. Res.* **2021**, *54*, 818–826.

(133) Askerka, M.; Brudvig, G. W.; Batista, V. S. The O_2-Evolving Complex of Photosystem II: Recent Insights from Quantum Mechanics/Molecular Mechanics (QM/MM), Extended X-ray Absorption Fine Structure (EXAFS), and Femtosecond X-ray Crystallography Data. *Acc. Chem. Res.* **2016**, *50*, 41–48.

(134) Siegbahn, P. E. M. Nucleophilic Water Attack Is Not a Possible Mechanism for O–O Bond Formation in Photosystem II. *Proc. Nat. Acad. Sci.* **2017**, *114*, 4966–4968.

(135) Ito, T.; Takagi, H.; Ishibashi, S.; Ido, T.; Uchida, S. Normal-State Conductivity Between CuO_2 Planes in Copper Oxide Superconductors. *Nature* **1991**, *350*, 596–598.

(136) Uemura, Y. J.; Luke, G. M.; Sternlieb, B. J.; Brewer, J. H.; Carolan, J. F.; Hardy, W.; Kadono, R.; Kempton, J. R.; Kiefl, R. F.; Kreitzman, S. R., et al. Universal Correlations Between T_c and $\frac{n_s}{m^*}$(Carrier Density Over Effective Mass) in High-T_c Cuprate Superconductors. *Phys. Rev. Lett.* **1989**, *62*, 2317.

TOC Graphic